Continuum Mech. Thermodyn.
https://doi.org/10.1007/s00161-023-01216-w

ORIGINAL ARTICLE

**Bülent Yagimli · Alexander Lion · Mohamed A. Abdelmoniem**

# Analytical investigation of the finite viscoelastic model proposed by Simo: critical review and a suggested modification

Received: 2 June 2022 / Accepted: 22 March 2023


**Abstract** Rubber components such as engine or suspension bearings are loaded during operation with large deformations and high-frequency loads. In industrial applications, finite element analysis software is therefore needed to simulate and predict the behaviour of these components under different scenarios of loading conditions. The usage of such software requires the user to be aware of certain limitations and shortcomings in the implemented material models. In this paper, the stresses as well as the storage and loss modulus are calculated analytically for an example of cyclic simple shear deformations. The analysed material model was firstly proposed by Simo and is available in Abaqus version 2018 for viscoelastic materials under finite strains. The analytical solution is used to highlight the non-physical response of the model under certain loading conditions. A modification of the modelling approach is then proposed to avoid such limitations. The modified model is implemented in the Abaqus software using a user material subroutine (UMAT). The behaviour of the modified model and the original Abaqus model are compared using an example of tie rod under different loading conditions. It is shown that with the suggested modification, reasonable results are obtained and the non-physical responses are eliminated.

**Keywords** Viscoelastic · Quasilinear viscoelastic · Frequency domain · Pre-load dependency

## 1 Introduction

The quasi-linear viscoelasticity[1] model also known as Fung's model is one of the most widely used models for finite viscoelasticity due to its simplicity. It was initially introduced by Fung to study the elongation behaviour of soft tissues [1]. The QLV model is a special form of the general Pipkin–Rogers model [2]. The stresses

[1] The quasi-linear viscoelasticity is abbreviated to QLV.

Communicated by Andreas Öchsner.

A. Lion and M. A. Abdelmoniem authors contributed equally to this work.

B. Yagimli (✉) · M. A. Abdelmoniem
Ostfalia University of Applied Science, Faculty of Mechanical Engineering, Salzdahlumer Straße 46/48, Wolfenbüttel 38302, Lower Saxony, Germany
E-mail: b.yagimli@ostfalia.de

M. A. Abdelmoniem
E-mail: m.abdelmoniem@ostfalia.de

A. Lion
Universität der Bundeswehr München, Faculty for Aerospace Engineering, Werner-Heisenberg-Weg 39, Neubiberg 85577, Bavaria, Germany
E-mail: alexander.lion@unibw.de

Published online: 22 April 2023

in this model are calculated by decreasing the instantaneous stress by an amount that depends on the past deformation history. A similar modelling approach was introduced by Simo [3], which is also commonly used and implemented in finite element method (FEM) software such as Abaqus 2018. Simo presents in [3] a material model to describe anisotropy, viscoelastic behaviour and continuum damage mechanics, known as Mullins' effect. The viscoelastic phenomena are based on a defined hyperelasticity model and a relaxation function.

Although the aforementioned models are widely used, they exhibit some deficiencies that have been discussed in several publications. In the work of Ciambella et al. [4], the predicted stress results of the QLV model were compared with the Abaqus model of finite viscoelasticity, presented in [5], section "Mechanical Constitutive Theories>Viscoelasticity>Finite-strain viscoelasticity". Main differences and certain shortcomings of the Abaqus model were highlighted. It was shown under simple shear loading that in comparison with the QLV model, the Abaqus model gives rise to normal stresses due to viscoelastic effects. This behaviour is non-physical and leads to an overestimation of the dissipated power. Using the same modelling approach as Ciambella et al. [4], a numerical method to compute the dissipated power involving the decomposition of the stretches and its FEM implementation was presented by Baaser [6]. The calculation of the dissipation was illustrated using an example of simple shear deformation. The plausibility of the results was checked, and the results were found to be reasonable.

The shortcomings of the QLV model were highlighted, and a modification was proposed in the published study by De Pascalis et al. [7]. The predictions of the introduced model were compared with the results from the model introduced by Ciambella et al. [4] and the model provided by Abaqus [5]. The results for a simple extension example showed a non-physical behaviour of Ciambella's model where an instantaneous zero stress was obtained whenever the stretch value recovers back to zero, which indicates no memory of the stress history.

In contrast to the above-mentioned models of finite viscoelasticity, different formulations, which are more suitable from the point of view of the thermodynamic consistency, were introduced by Lion [8], Reese and Govindjee [9], Haupt and Lion [10]. Based on the model in [10], modified formulations were presented in [11], [12], and [13] to model, for example, the kinetics of curing of epoxy. A multiplicative split of deformation gradient was proposed by Lion [8] and [9] for a finite viscoelastic model. This model was implemented by Johlitz et al. [14] and Schröder et al. [15] to analyse the dissipative self-heating in elastomers.

A phenomenological inelastic constitutive model for rubber-like materials (MORPH model) was presented by Besdo and Ihlemann [16] to describe the damage mechanics of elastomers. The model uses eight material parameters to model several effects such as hysteresis, softening, and residual strains. The MORPH model was used by Juhre et al. [17] to discuss the effect of inelasticity on the fatigue life of filled elastomers and was recently used by Weiser et al. [18] to model the mechanical behaviour of cord-elastomer composites.

On the micro-mechanical level using the transient network theory, a finite viscoelastic model, which is based on the multiplicative decomposition of the deformation gradient, was introduced by Reese [19]. A physically motivated micro-mechanical model referred to as the non-affine micro-sphere model was presented by Miehe et al. [20]. Using cluster mechanics, the dynamic flocculation model (DFM model) was presented by Raghunath et al. [21]. The DFM model is based on the non-affine tube model and is able to model the softening behaviour as well as the hysteresis during quasi-static experiments. It requires, however, the use of the concept of representative directions to be implemented in FEM programs. The concept of representative direction generalised one-dimensional material models to three-dimensional constitutive models, which is introduced by Freund and Ihlemann [22]. Plagge et al. [23] modified and extended the DFM model to a mathematically more robust approach (SIRM model). The model requires seven to nine parameters to cover almost the full phenomenology of filled rubber. The authors, however, highlighted some shortcomings in the introduced approach such as the thermodynamic consistency of the Prony element. A recent three-parameter micro-mechanical model was presented by Dal et al. [24]. The model is an extension to the well-known eight-chain model, proposed by Arruda and Boyce [25]. By adding a second invariant-based energy term, the eight-chain model is enhanced under biaxial deformation.

Based on the principles of Boltzmann [26], the fading memory of viscoelastic materials can be modelled with a convolution integral. A special form of the convolution integral proposed by Fung [1] is known as quasi-linear viscoelastic model (QLV). The focus of this article is on the model with internal variables provided by Simo [3] (Simo model). The Simo model approach is very similar to the QLV model and is widely used in FEM software to model the viscoelastic behaviour of materials in a vast variety of applications. Behnke and Kaliske [27] used the Simo model to perform a thermomechanical coupled simulation of rolling tires under steady-state conditions. The dissipated energy due to viscoelastic effects was computed, and the surface temperature of the tire was compared to experimental results. The model showed promising predictability in a wide range

of testing scenarios. In the work of Berjamin et al. [28], the QLV model was linked with the Simo model by incorporating a single scalar relaxation function in the QLV model. The new approach was referred to by the authors as the 'Fung-Simo' model. The thermodynamic consistency of the new model (Fung-Simo model) was illustrated, and the dissipative features were presented in an example of simple tension. In a recent article by Berjamin and De Pascalis [29], the Fung-Simo model was used in an acoustoelastic analysis of phononic crystals. In the biomedical field, the QLV model is confirmed to be a reasonable model for a wide range of materials. It was used, for example, by Rashid et al. [30] to model brain tissues under dynamic strains and by Lucas et al. to evaluate the linear viscoelastic behaviour of cervical spinal ligaments under fast-rate loading [31]. As discussed by De Pascalis [7], the QLV model was implemented in the literature with other variant forms that are slightly different from the original model proposed by Fung.

In this paper, the model presented by Simo [3] and implemented in the FEM Software Abaqus 2018 is discussed analytically. The analytical solution of the model is derived using an example of simple shear deformation. As shown in [32], it has to be highlighted that the boundary value problem of simple shear is, even for elasticity, a complex problem. In many studies [7,30,33], and [34], simple shear is used to demonstrate the capability of a material model. Using the analytical solution, the resulting terms lead to the non-physical behaviour of the model. These undesired behaviours are, for example, the overshoot oscillation at certain frequencies, the pre-deformation dependency, and the amplitude dependency of the model. Furthermore, a modification of the model is suggested to eliminate the sources of the non-physical behaviour. After discussing the analytical solution, the modified model is programmed using the programming language Fortran 77 and implemented in the Abaqus software through the user material subroutine (UMAT). Finally, an FEM simulation is performed on an example of a tie rod under different loading scenarios. The FEM implementation aims to highlight the existing shortcomings in the current Abaqus implementation and how they were overcame using the modified model.

## 2 Viscoelasticity model for finite deformation

### 2.1 Principle of the finite viscoelastic Simo model

The presented model is motivated by generalised Maxwell elements (s. [35, p. 337]). A complete definition of the free energy function is required to ensure thermodynamic consistency. An additive split into equilibrium and non-equilibrium parts is suggested:

$$\rho_0 \Psi = \rho_0 \Psi_{\mathrm{eq}}(\mathbf{C}, \theta) + \rho_0 \Psi_{\mathrm{neq}}(\bar{\mathbf{C}}, \tilde{\mathbf{T}}_{\mathrm{ov},k}, \theta) \tag{1}$$

Herein the initial density is given as $\rho_0$ and $\theta$ is the temperature. The non-equilibrium part of the free energy is dependent on the unimodular right Cauchy–Green tensor.[2] It is assumed that the volumetric deformation leads only to a change in the equilibrium part of the free energy. The internal variables $\tilde{\mathbf{T}}_{\mathrm{ov},k}$ represent the inelastic behaviour for each Maxwell element. Based on the treatments of Flory in [36], the volumetric and isochoric deformation can be isolated from each other with an additive split of the free energy and a multiplicative split of the deformation gradient

$$\rho_0 \Psi_{\mathrm{eq}} = U^{\circ}(J, \theta) + \gamma_{\infty} \bar{W}^{\circ}(\bar{\mathbf{C}}, \theta) + \rho_0 \Psi_{\mathrm{th}}(\theta). \tag{2}$$

Herein $U^{\circ}$ and $\bar{W}^{\circ}$ are the specific hyperelastic energy functions per volume for instantaneous deformation processes. In the following, all variables for instantaneous deformation processes are signed with $(\bullet)^{\circ}$. The non-equilibrium part of the free energy is defined as:

$$\rho_0 \Psi_{\mathrm{neq}}(\bar{\mathbf{C}}, \tilde{\mathbf{T}}_{\mathrm{ov},k}, \theta) = \sum_{k=1}^{N} \gamma_k \tilde{\mathbf{T}}_{\mathrm{ov},k} : \frac{1}{2}\bar{\mathbf{C}} + \Xi \left( \sum_{k=1}^{N} \tilde{\mathbf{T}}_{\mathrm{ov},k} \right). \tag{3}$$

The last term is defined in the equilibrium state, where the rates of the internal variables are zero. A Legendre transformation of the internal variable $\tilde{\mathbf{T}}_{\mathrm{ov},k}$ and the associated internal variable as deformation tensor is suggested at this point in [35, p. 351, Eq. 10.2.22]. In [35, p. 351] and [27], a definition in the equilibrium state

[2] The well-known variables of continuum mechanics and some tensor operators are listed in Table 1.

**Table 1** Notations

| ID | Symbol | Calculation | Description |
|---|---|---|---|
| | *Deformation variables* | | |
| 1 | $\mathbf{F}$ | | Deformation gradient |
| 2 | $J$ | $\det(\mathbf{F})$ | Determinant of the deformation gradient |
| 3 | $\bar{\mathbf{F}}$ | $J^{-\frac{1}{3}}\mathbf{F}$ | Unimodular deformation gradient |
| 3 | $\mathbf{C}$ | $\mathbf{F}^T\mathbf{F}$ | Right Cauchy–Green tensor |
| 4 | $\bar{\mathbf{C}}$ | $J^{-\frac{2}{3}}\mathbf{C}$ | Unimodular right Cauchy–Green tensor |
| 5 | $\mathbf{B}$ | $\mathbf{F}\mathbf{F}^T$ | left Cauchy–Green tensor |
| 6 | $\bar{\mathbf{B}}$ | $J^{-\frac{2}{3}}\mathbf{B}$ | Unimodular left Cauchy–Green tensor |
| | *Stress-like tensors* | | |
| 7 | $\tilde{\mathbf{T}}$ | | 2nd Piola–Kirchhoff stress tensor |
| 8 | $\mathbf{T}$ | $J^{-1}\mathbf{F}\tilde{\mathbf{T}}\mathbf{F}^T$ | Cauchy stress tensor |
| 9 | $\mathbf{S}$ | $\mathbf{F}\tilde{\mathbf{T}}\mathbf{F}^T$ | Weighted Cauchy stress tensor |
| 10 | $\tilde{\mathbf{T}}_{\text{iso}}$ | | Isochoric 2nd Piola–Kirchhoff stress tensor |
| 11 | $\mathbf{T}_{\text{iso}}$ | $J^{-1}\bar{\mathbf{F}}\tilde{\mathbf{T}}_{\text{iso}}\bar{\mathbf{F}}^T$ | Isochoric Cauchy stress tensor |
| 12 | $\tilde{\mathbf{T}}^{\circ}_{\text{iso}}$ | | Isochoric 2nd Piola–Kirchhoff stress tensor for instantaneous load history |
| 13 | $\mathbf{S}_{\text{iso}}$ | $\bar{\mathbf{F}}\tilde{\mathbf{T}}_{\text{iso}}\bar{\mathbf{F}}^T$ | Weighted isochoric Cauchy stress tensor |
| 14 | $\tilde{\mathbf{T}}_{\text{ov}}$ | | Overstress 2nd Piola–Kirchhoff stress tensor |
| 15 | $\tilde{\mathbf{T}}_{\text{ov},k}$ | | Overstress 2nd Piola–Kirchhoff stress tensor for $k$-th Maxwell element |
| 16 | $\mathbf{T}_{\text{ov}}$ | $J^{-1}\bar{\mathbf{F}}\tilde{\mathbf{T}}_{\text{ov}}\bar{\mathbf{F}}^T$ | Overstress Cauchy stress tensor |
| 17 | $\mathbf{S}_{\text{ov}}$ | $\bar{\mathbf{F}}\tilde{\mathbf{T}}_{\text{ov}}\bar{\mathbf{F}}^T$ | Weighted overstress Cauchy stress tensor |
| | *Energy variables* | | |
| 18 | $\Psi$ | $\Psi(\mathbf{C}(t),\theta(t))$ | Free energy |
| 19 | $\Psi_{\text{eq}}$ | $\Psi_{\text{eq}}(\mathbf{C},\theta)$ | Equilibrium free energy |
| 20 | $\Psi_{\text{th}}$ | $\Psi_{\text{th}}(\theta)$ | Thermal free energy |
| 21 | $\Psi_{\text{neq}}$ | $\Psi_{\text{neq}}(\bar{\mathbf{C}}(t),\theta(t))$ | Non-equilibrium free energy |
| 22 | $\bar{W}^{\circ}$ | $\bar{W}^{\circ}(\bar{\mathbf{C}},\theta)$ | Isochoric stored energy for instantaneous load history |
| 23 | $U^{\circ}$ | $U^{\circ}(J,\theta)$ | Volumetric stored energy for instantaneous load history |
| | *Mathematical operations:* | | |
| 24 | $\text{DEV}\,[(\bullet)] = (\bullet) - \frac{1}{3}\left((\bullet)\cdot\mathbf{C}\right)\mathbf{C}^{-1}$ | | Deviator operator in initial configuration |
| 25 | $\overline{\text{DEV}}\,[(\bullet)] = J^{-\frac{2}{3}}\left[(\bullet) - \frac{1}{3}\left((\bullet)\cdot\mathbf{C}\right)\mathbf{C}^{-1}\right]$ | | Deviator operator in intermediate isochoric configuration |
| 26 | $\text{dev}\,[(\bullet)] = (\bullet) - \frac{1}{3}\left((\bullet)\cdot\mathbf{1}\right)\mathbf{1}$ | | Deviator operator in current configuration |

is suggested. In Eq. (3), the parameter $\gamma_k$ is the proportionality factor for the k-th Maxwell element. Through this formulation of the free energy, a potential relation for the 2nd Piola–Kirchhoff stress tensor can be derived

$$\tilde{\mathbf{T}} = 2\rho_0 \frac{\partial \Psi}{\partial \mathbf{C}} = 2\rho_0 \partial_{\mathbf{C}} \Psi. \tag{4}$$

For the sake of clarity, partial derivatives are written as $\frac{\partial \Psi}{\partial \mathbf{C}} = \partial_{\mathbf{C}}\Psi$, so that the 2nd Piola–Kirchhoff stress tensor results in

$$\begin{aligned}\tilde{\mathbf{T}} = \partial_J U^{\circ} J\mathbf{C}^{-1} + \gamma_{\infty} J^{-\frac{2}{3}}\left(\partial_{\bar{\mathbf{C}}}\bar{W}^{\circ} - \frac{1}{3}\left(\mathbf{C} : \partial_{\bar{\mathbf{C}}}\bar{W}^{\circ}\right)\mathbf{C}^{-1}\right)\\ + \sum_{k=1}^{N}\gamma_k J^{-\frac{2}{3}}\left(\tilde{\mathbf{T}}_{\text{ov},k} - \frac{1}{3}\left(\mathbf{C} : \tilde{\mathbf{T}}_{\text{ov},k}\right)\mathbf{C}^{-1}\right).\end{aligned} \tag{5}$$

In [35, p. 360 Eq. (10.4.12)], a deviatoric operator in the initial configuration is defined as:

$$\text{DEV}\,[(\bullet)] = (\bullet) - \frac{1}{3}(\mathbf{C} : (\bullet))\mathbf{C}^{-1} \tag{6}$$

with the property

$$\mathbf{F}\text{DEV}\,[(\bullet)]\,\mathbf{F}^T = \mathbf{F}(\bullet)\mathbf{F}^T - \frac{1}{3}(\mathbf{1} : \mathbf{F}(\bullet)\mathbf{F}^T)\mathbf{1} = \text{dev}\left[\mathbf{F}(\bullet)\mathbf{F}^T\right]. \tag{7}$$

An enhanced deviatoric operator can be defined as:

$$\overline{\mathrm{DEV}}\left[(\bullet)\right] = J^{-\frac{2}{3}}\left((\bullet) - \frac{1}{3}(\mathbf{C} : (\bullet))\mathbf{C}^{-1}\right) \tag{8}$$

with

$$\mathbf{F}\overline{\mathrm{DEV}}\left[(\bullet)\right]\mathbf{F}^T = \bar{\mathbf{F}}(\bullet)\bar{\mathbf{F}}^T - \frac{1}{3}(\mathbf{1} : \bar{\mathbf{F}}(\bullet)\bar{\mathbf{F}}^T)\mathbf{1} = \mathrm{dev}\left[\bar{\mathbf{F}}(\bullet)\bar{\mathbf{F}}^T\right]. \tag{9}$$

Since the arguments in the deviatoric operator are linear, the 2nd Piola–Kirchhoff stress tensor is given as:

$$\tilde{\mathbf{T}} = \partial_J U^\circ J\mathbf{C}^{-1} + \overline{\mathrm{DEV}}\left[\gamma_\infty 2\partial_{\bar{\mathbf{C}}}\bar{W}^\circ + \sum_{k=1}^{N}\gamma_k\tilde{\mathbf{T}}_{\mathrm{ov},k}\right]. \tag{10}$$

The following partial derivative of the instantaneous stored energy function is defined as a stress-like source term:

$$\tilde{\mathbf{T}}^\circ_{\mathrm{iso}} = 2\partial_{\bar{\mathbf{C}}}\bar{W}^\circ. \tag{11}$$

Thus, the 2nd Piola–Kirchhoff stress tensor is given as:

$$\tilde{\mathbf{T}} = J\partial_J U^\circ\mathbf{C}^{-1} + \overline{\mathrm{DEV}}\left[\gamma_\infty\tilde{\mathbf{T}}^\circ_{\mathrm{iso}} + \sum_{k=1}^{N}\gamma_k\tilde{\mathbf{T}}_{\mathrm{ov},k}\right]. \tag{12}$$

In [35, p. 365 Eq. (10.5.2)], Simo and Hughes recommend an evolution equation for the overstress, which is motivated from the rheological 1D-Maxwell element. This idea transformed to the equation introduced in Eq. (3), which leads to the following evolution equation

$$\dot{\tilde{\mathbf{T}}}_{\mathrm{ov},k} + \frac{1}{\tau_k}\tilde{\mathbf{T}}_{\mathrm{ov},k} = \frac{\mathrm{d}}{\mathrm{d}t}\left(\overline{\mathrm{DEV}}\left[\tilde{\mathbf{T}}^\circ_{\mathrm{iso}}\right]\right). \tag{13}$$

Herein the time derivative is signed with $(\dot{\bullet}) = \frac{\mathrm{d}}{\mathrm{d}t}(\bullet)$. This evolution equation can be transformed to a convolution integral

$$\tilde{\mathbf{T}}_{\mathrm{ov},k} = \int_{-\infty}^{t} e^{-\frac{t-s}{\tau_k}}\frac{\mathrm{d}}{\mathrm{d}s}\left(\overline{\mathrm{DEV}}\left[\tilde{\mathbf{T}}^\circ_{\mathrm{iso}}(s)\right]\right)\mathrm{d}s. \tag{14}$$

Therefore, the weighted Cauchy stress tensor is defined with the forward transformation of the 2nd Piola–Kirchhoff stress tensor (see eqs. (5) and (14))

$$\mathbf{S} = \mathbf{F}\tilde{\mathbf{T}}\mathbf{F}^T = J\partial_J U^\circ\mathbf{1} + \mathrm{dev}\left[\gamma_\infty\underbrace{\bar{\mathbf{F}}\tilde{\mathbf{T}}^\circ_{\mathrm{iso}}\bar{\mathbf{F}}^T}_{\mathbf{S}^\circ_{\mathrm{iso}}} + \sum_{k=1}^{N}\gamma_k\underbrace{\bar{\mathbf{F}}\tilde{\mathbf{T}}_{\mathrm{ov},k}\bar{\mathbf{F}}^T}_{\mathbf{S}_{\mathrm{ov},k}}\right] \tag{15}$$

$$\mathbf{S} = J\partial_J U^\circ\mathbf{1} + \gamma_\infty\mathrm{dev}\left[\mathbf{S}^\circ_{\mathrm{iso}}\right] + \sum_{k=1}^{N}\gamma_k\mathrm{dev}\underbrace{\left[\bar{\mathbf{F}}\int_{-\infty}^{t} e^{-\frac{t-s}{\tau_k}}\frac{\mathrm{d}}{\mathrm{d}s}\left(\overline{\mathrm{DEV}}\left[\tilde{\mathbf{T}}^\circ_{\mathrm{iso}}(s)\right]\right)\mathrm{d}s\bar{\mathbf{F}}^T\right]}_{\mathbf{S}_{\mathrm{ov},k}}. \tag{16}$$

For a nearly static load history, the overstress part is $\tilde{\mathbf{T}}_{\mathrm{ov},k} \approx \mathbf{0}$ and consequently $\mathbf{S}_{\mathrm{ov},k} \approx \mathbf{0}$. In this case, the weighted Cauchy stress tensor is approximated to:

$$\mathbf{S} \approx \partial_J U^\circ J\mathbf{1} + \gamma_\infty\mathrm{dev}\left[\mathbf{S}^\circ_{\mathrm{iso}}\right]. \tag{17}$$

**Table 2** Definition of finite proportional viscoelasticity

| | |
|---|---|
| *Known or accordingly given functions* | |
| Instantaneous stored isochoric energy | $\bar{W}^{\circ}(\bar{\mathbf{C}})$ |
| Instantaneous stored volumetric energy | $U^{\circ}(J)$ |
| Relaxation function with relative coefficients | $g(t) = \gamma_{\infty} + \sum_{k=1}^{N} \gamma_k e^{-\frac{t}{\tau_k}}$ |
| *Variables, which have to be defined with respect to deformation history* | |
| Instantaneous isochoric 2nd Piola–Kirchhoff stress tensor | $\tilde{\mathbf{T}}^{\circ}_{\text{iso}} = 2\partial_{\bar{\mathbf{C}}}\bar{W}^{\circ}$ |
| Instantaneous isochoric weighted Cauchy stress tensor | $\mathbf{S}^{\circ}_{\text{iso}} = \bar{\mathbf{F}}\tilde{\mathbf{T}}^{\circ}_{\text{iso}}\bar{\mathbf{F}}^{T}$ |
| Overstress of weighted Cauchy tensor | $\mathbf{S}_{\text{ov},k} = \bar{\mathbf{F}} \int_{-\infty}^{t} e^{-\frac{t-s}{\tau_k}} \frac{\mathrm{d}}{\mathrm{d}s} \left( \overline{\text{DEV}} \left[ \tilde{\mathbf{T}}^{\circ}_{\text{iso}} \right] \right) \mathrm{d}s \bar{\mathbf{F}}^{T}$ |
| Weighted Cauchy stress tensor | $\mathbf{S} = J\partial_J U^{\circ}\mathbf{1} + \text{dev}\left[\gamma_{\infty}\mathbf{S}^{\circ}_{\text{iso}} + \sum_{k=1}^{N} \gamma_k \mathbf{S}_{\text{ov},k}\right]$ |
| **S** with relaxation function | $\mathbf{S} = J\partial_J U^{\circ}\mathbf{1} + \text{dev}\left[\bar{\mathbf{F}} \int_{-\infty}^{t} g(t-s) \frac{\mathrm{d}}{\mathrm{d}s} \left( \overline{\text{DEV}} \left[ \tilde{\mathbf{T}}^{\circ}_{\text{iso}} \right] \right) \mathrm{d}s \bar{\mathbf{F}}^{T}\right]$ |

In the case of an instantaneous deformation with a high rate, the weighted Cauchy stress tensor is:

$$\mathbf{S} \approx \partial_J U^{\circ} J\mathbf{1} + \left( \gamma_{\infty} + \sum_{k=1}^{N} \gamma_k \right) \text{dev}\left[\mathbf{S}^{\circ}_{\text{iso}}\right]. \tag{18}$$

The main idea of the proportional viscoelasticity is that the weighted Cauchy stress tensor **S** can be defined with stress tensor $\mathbf{S}^{\circ}_{\text{iso}}$ in case of instantaneous deformation processes

$$\mathbf{S} \approx \partial_J U^{\circ} J\mathbf{1} + \text{dev}\left[\mathbf{S}^{\circ}_{\text{iso}}\right]. \tag{19}$$

This motivation leads to the restriction

$$1 = \gamma_{\infty} + \sum_{k=1}^{N} \gamma_k. \tag{20}$$

It has to be checked whether this also applies to cyclic deformations with high deformation rates.

The stress equations are summarised in Table 2. The equilibrium part of the weighted Cauchy stress tensor is proportional with the parameter $\gamma_{\infty}$ to the instantaneous weighted Cauchy tensor. This type of finite viscoelasticity is assigned as a proportional energy function represented in [37]. To model the finite viscoelastic behaviour, two constitutive functions are needed. On the one hand, a hyperelastic energy function and on the other hand an exponential series with relative moduli $\gamma_i$ and corresponding relaxation times $\tau_i$, which is also known as the Prony series. The suggested evolution equation doesn't satisfy the request in Eq. (18) entirely. This is discussed in the next section.

## 2.2 Simo model with neo-Hookean hyperelasticity

For the sake of clarity, in the following only one Maxwell element is assumed and a neo-Hookean hyperelasticity model is assumed for the stored energy function

$$U^{\circ} = \frac{\kappa}{2} (\ln(J))^2 \quad \text{and} \quad \bar{W}^{\circ} = c_{10} \left( I_{\bar{\mathbf{C}}} - 3 \right). \tag{21}$$

Herein $I_{\bar{\mathbf{C}}}$ is the first invariant of the unimodular right Cauchy–Green tensor. Usually for isotropic hyperelasticity, the stored energy function depends on the first invariant

$$I_{\bar{\mathbf{C}}} = \bar{\mathbf{C}} : \mathbf{1} \tag{22}$$

and the second invariant

$$I I_{\bar{\mathbf{C}}} = \tfrac{1}{2} \left( (\bar{\mathbf{C}} : \mathbf{1})^2 - \bar{\mathbf{C}}\bar{\mathbf{C}} : \mathbf{1} \right). \tag{23}$$

In case of neo-Hookean elasticity, the stored energy $\bar{W}^{\circ}$ is only a function of the first invariant. Hence, the instantaneous 2nd Piola–Kirchhoff stress tensor according to Eq. (11) is

$$\tilde{\mathbf{T}}^{\circ}_{\mathrm{iso}} = 2c_{10}\mathbf{1}. \tag{24}$$

Therefore, the overstress part is determined by:

$$\dot{\tilde{\mathbf{T}}}_{\mathrm{ov}} + \frac{1}{\tau}\tilde{\mathbf{T}}_{\mathrm{ov}} = 2c_{10}\frac{\mathrm{d}}{\mathrm{d}t}\left(\overline{\mathrm{DEV}}\,[\mathbf{1}]\right). \tag{25}$$

To understand the relation between the deformation history and the stress tensor, the weighted Cauchy stress tensor is derived for a simple shear oscillation:

$$\mathbf{F} = \begin{bmatrix} 1 & \alpha(t) & 0 \\ 0 & 1 & 0 \\ 0 & 0 & 1 \end{bmatrix}. \tag{26}$$

For orthogonal base vectors, the deformation gradient can be represented by a $3 \times 3$ matrix. Herein $\alpha(t)$ is the shear angle function, which oscillates with the angular frequency $\omega$ and the amplitude $\hat{\alpha}$

$$\alpha(t) = \hat{\alpha}\sin(\omega t). \tag{27}$$

The deformation gradient (26) inserted in Eq. (25) with Eq. (8) yields to

$$\begin{aligned} \dot{\tilde{\mathbf{T}}}_{\mathrm{ov}} + \frac{1}{\tau}\tilde{\mathbf{T}}_{\mathrm{ov}} &= 2c_{10}\frac{\mathrm{d}}{\mathrm{d}t}\left(\begin{bmatrix} -\left(\frac{4\alpha^2}{3} + \frac{\alpha^4}{3}\right) & \left(\alpha + \frac{\alpha^3}{3}\right) & 0 \\ \left(\alpha + \frac{\alpha^3}{3}\right) & -\frac{\alpha^2}{3} & 0 \\ 0 & 0 & -\frac{\alpha^2}{3} \end{bmatrix}\right) \\ \dot{\tilde{\mathbf{T}}}_{\mathrm{ov}} + \frac{1}{\tau}\tilde{\mathbf{T}}_{\mathrm{ov}} &= 2c_{10}\begin{bmatrix} -\left(\frac{8\alpha\dot{\alpha}+4\alpha^3\dot{\alpha}}{3}\right) & \left(\dot{\alpha} + \dot{\alpha}\alpha^2\right) & 0 \\ \left(\dot{\alpha} + \dot{\alpha}\alpha^2\right) & -\frac{2\dot{\alpha}\alpha}{3} & 0 \\ 0 & 0 & -\frac{2\dot{\alpha}\alpha}{3} \end{bmatrix}. \end{aligned} \tag{28}$$

With the given shear oscillation (27), the differentiation can be carried out. Every product of sine and cosine functions can be transformed to a linear sine and cosine function with a corresponding frequency. Thus, each component of the overstress tensor $\tilde{\mathbf{T}}_{\mathrm{ov}}$ is determined by a non-homogeneous ordinary differential equation:

$$\left[\dot{\tilde{\mathbf{T}}}_{\mathrm{ov}}\right]_{ij} + \frac{1}{\tau}\left[\tilde{\mathbf{T}}_{\mathrm{ov}}\right]_{ij} = \sum_{l=1}^{n} l\omega\left(A_{ij,l}\cos(l\omega t) + B_{ij,l}\sin(l\omega t)\right). \tag{29}$$

The terms $A_{ij,l}$ and $B_{ij,l}$ are the amplitudes for the corresponding frequency $l\omega$ and can be calculated from the right-hand side of equation (28)

$$B_{11,2} = -2c_{10}\frac{\hat{\alpha}^4 + 4\hat{\alpha}^2}{6} \quad \text{and} \quad B_{11,4} = 2c_{10}\frac{\hat{\alpha}^4}{24}, \tag{30}$$

$$B_{22,2} = B_{33,2} = -2c_{10}\frac{\hat{\alpha}^2}{6}, \tag{31}$$

$$A_{12,1} = 2c_{10}\left(\hat{\alpha} + \frac{\hat{\alpha}^3}{4}\right) \quad \text{and} \quad A_{12,3} = -2c_{10}\frac{\hat{\alpha}^3}{4}. \tag{32}$$

All other coefficients are zero. The solution of this first-order differential equation is:

$$\begin{aligned} \left[\tilde{\mathbf{T}}_{\mathrm{ov}}\right]_{ij} = C_{ij}e^{-\frac{t}{\tau}} + \sum_{l=1}^{n}\frac{l\tau\omega}{1 + (l\tau\omega)^2}\big[&(B_{ij,l} + l\tau\omega A_{ij,l})\sin(l\omega t) \\ &+ (A_{ij,l} - l\tau\omega B_{ij,l})\cos(l\omega t)\big]. \end{aligned} \tag{33}$$

**Table 3** Definition of finite proportional viscoelasticity with neo-Hookean hyperelasticity

| | |
|---|---|
| *Known or accordingly given functions* | |
| Instantaneous stored isochoric energy: | $\bar{W}^{\circ}(\bar{\mathbf{C}}) = c_{10}(I_{\bar{\mathbf{C}}} - 3)$ |
| Instantaneous stored volumetric energy: | $U^{\circ}(J) = \frac{\kappa}{2}\left(\ln(J)\right)^2$ |
| Relaxation function with relative coefficients: | $g(t) = \gamma_{\infty} + \sum_{k=1}^{N} \gamma_k e^{-\frac{t}{\tau_k}}$ |
| *Variables, which have to be defined with respect to deformation history* | |
| Instantaneous isochoric 2nd Piola–Kirchhoff stress tensor: | $\tilde{\mathbf{T}}^{\circ}_{\text{iso}} = 2c_{10}\mathbf{1}$ |
| Instantaneous isochoric weighted Cauchy stress tensor: | $\mathbf{S}^{\circ}_{\text{iso}} = 2c_{10}\bar{\mathbf{B}}$ |
| Overstress of weighted Cauchy stress tensor: | $\mathbf{S}_{\text{ov},k} = \bar{\mathbf{F}} \int_{-\infty}^{t} 2c_{10} e^{-\frac{t-s}{\tau_k}} \frac{\mathrm{d}}{\mathrm{d}s}\left(\overline{\text{DEV}}\left[\mathbf{1}\right]\right) \mathrm{d}s \bar{\mathbf{F}}^T$ |
| Weighted Cauchy stress tensor | $\mathbf{S} = \kappa \ln(J)\mathbf{1} + \text{dev}\left[\gamma_{\infty}\mathbf{S}^{\circ}_{\text{iso}} + \sum_{k=1}^{N} \gamma_k \mathbf{S}_{\text{ov},k}\right]$ |

With the initial condition $\tilde{\mathbf{T}}_{\text{ov}}(t=0) = \mathbf{0}$, the integration constants $C_{ij}$ can be calculated. Since the overstress part of 2nd Piola–Kirchhoff stress tensor is already computed, the weighted Cauchy stress tensor is obtained with the pushforward operation (see Eq. (15))

$$\mathbf{S} = J\partial_J U^{\circ}\mathbf{1} + \text{dev}\left[\gamma_{\infty}\mathbf{S}^{\circ}_{\text{iso}} + \gamma\mathbf{S}_{\text{ov}}\right]. \tag{34}$$

The chosen hyperelasticity function leads to:

$$\mathbf{S}^{\circ}_{\text{iso}} = 2c_{10}\bar{\mathbf{B}}. \tag{35}$$

With the solution (33) and the definition in Eq. (15), the overstress part of the weighted Cauchy stress tensor is defined. The derived equations to define the weighted Cauchy stress tensor are summarised in Table 3. The response function for each component of $\mathbf{S}_{\text{ov}}$ is as follows:

$$[\mathbf{S}_{\text{ov}}]_{11} = a_{11,0} + \sum_{l=1}^{4}\left(a_{11,l}\cos(l\omega t) + b_{11,l}\sin(l\omega t)\right), \tag{36}$$

with the coefficients

$$\begin{aligned}
a_{11,0} &= c_{10}\hat{\alpha}^2\bar{\omega}^2\left(\frac{(4+\hat{\alpha}^2)}{2(1+\bar{\omega}^2)} - \frac{\hat{\alpha}^2}{3\left(1+(3\bar{\omega})^2\right)} - \frac{16+6\hat{\alpha}^2}{3\left(1+(2\bar{\omega})^2\right)}e^{-\frac{t}{\tau}}\right.\\
&\quad\left. + \frac{4\hat{\alpha}^2}{\left(1+(4\bar{\omega})^2\right)}e^{-\frac{t}{\tau}}\right),\\
b_{11,1} &= c_{10}\hat{\alpha}^2\bar{\omega}e^{\frac{t}{\tau}}\left(\frac{\hat{\alpha}^2}{1+(3\bar{\omega})^2} - \frac{(4+\hat{\alpha}^2)}{1+\bar{\omega}^2}\right),\\
a_{11,2} &= c_{10}\hat{\alpha}^2\bar{\omega}^2\left(\frac{4(4+\hat{\alpha}^2)}{3\left(1+(2\bar{\omega})^2\right)} + \frac{2\hat{\alpha}^2}{3\left(1+(2\bar{\omega})^2\right)}\left(1+e^{-\frac{t}{\tau}}\right)\right.\\
&\quad\left. - \frac{4+\hat{\alpha}^2}{2(1+\bar{\omega}^2)} - \frac{3\hat{\alpha}^2}{2\left(1+(3\bar{\omega})^2\right)}\right),\\
b_{11,2} &= c_{10}\hat{\alpha}^2\bar{\omega}\left(-\frac{(8+3\hat{\alpha}^2)}{3\left(1+(2\bar{\omega})^2\right)} + \frac{4+\hat{\alpha}^2}{2(1+\bar{\omega}^2)} + \frac{\hat{\alpha}^2}{2\left(1+(3\bar{\omega})^2\right)}\right),\\
a_{11,4} &= c_{10}\hat{\alpha}^4\bar{\omega}^2\left(-\frac{4}{3\left(1+(4\bar{\omega})^2\right)} - \frac{1}{3(1+(2\bar{\omega})^2)} + \frac{3}{2(1+(3\bar{\omega})^2)}\right),\\
b_{11,4} &= c_{10}\hat{\alpha}^4\bar{\omega}\left(\frac{4}{3\left(1+(4\bar{\omega})^2\right)} + \frac{1}{6(1+(2\bar{\omega})^2)} - \frac{1}{2(1+(3\bar{\omega})^2)}\right)
\end{aligned} \tag{37}$$

and

$$a_{11,1} = a_{11,3} = b_{11,3} = 0.$$

Herein, a relative angular frequency $\bar{\omega} = \omega\tau$ is introduced. The shear stress component is as follows:

$$[\mathbf{S}_{\mathrm{ov}}]_{12} = a_{12,0} + \sum_{l=1}^{3} \left( a_{12,l} \cos(l\omega t) + b_{12,l} \sin(l\omega t) \right), \tag{38}$$

with the coefficients

$$\begin{aligned}
a_{12,0} &= c_{10}\bar{\omega}\hat{\alpha} e^{-\frac{t}{\tau}} \left( -\frac{4+\hat{\alpha}^2}{2(1+\bar{\omega}^2)} + \frac{\hat{\alpha}^2}{2(1+(3\bar{\omega})^2)} \right), \\
a_{12,1} &= c_{10}\bar{\omega}\hat{\alpha} \left( \frac{4+\hat{\alpha}^2}{2(1+\bar{\omega}^2)} - \frac{\hat{\alpha}^2}{3(1+(2\bar{\omega})^2)} \right), \\
b_{12,1} &= c_{10}\bar{\omega}^2\hat{\alpha} \left( \frac{4+\hat{\alpha}^2}{2(1+\bar{\omega}^2)} - \frac{2\hat{\alpha}^2}{3(1+(2\bar{\omega})^2)} \left(1 + 2e^{-\frac{t}{\tau}}\right) \right), \\
a_{12,3} &= c_{10}\bar{\omega}\hat{\alpha}^3 \left( -\frac{1}{2(1+(3\bar{\omega})^2)} + \frac{1}{3(1+(2\bar{\omega})^2)} \right), \\
b_{12,3} &= c_{10}\bar{\omega}^2\hat{\alpha}^3 \left( -\frac{3}{2(1+(3\bar{\omega})^2)} + \frac{2}{3(1+(2\bar{\omega})^2)} \right)
\end{aligned}$$

and

$$a_{12,2} = b_{12,2} = 0.$$

Furthermore, the diagonal components are given as:

$$[\mathbf{S}_{\mathrm{ov}}]_{22} = [\mathbf{S}_{\mathrm{ov}}]_{33} = -\frac{2c_{10}^{\circ}\hat{\alpha}^2\bar{\omega}}{3\left(1+(2\bar{\omega})^2\right)} \left( \sin(2\omega t) - 2\bar{\omega} \left( \cos(2\omega t) - e^{-\frac{t}{\tau}} \right) \right) \tag{39}$$

For a very small relative angular frequency $\bar{\omega} \ll 1$, the overstress converges to:

$$\bar{\omega} \ll 1 \text{ and } t \gg \tau \quad \Rightarrow \quad \mathbf{S}_{\mathrm{ov}} \approx \mathbf{0} \tag{40}$$

and therefore

$$\bar{\omega} \ll 1 \text{ and } t \gg \tau \quad \Rightarrow \quad \mathbf{S} \approx J\partial_J U^{\circ}\mathbf{1} + \gamma_{\infty} 2c_{10}\mathrm{dev}\left[\bar{\mathbf{B}}\right]. \tag{41}$$

For a very high relative angular frequency $\bar{\omega}$, the amplitudes $a_{11,4}$, $b_{11,4}$, $a_{12,0}$, $a_{12,1}$ and $a_{12,3}$, $b_{12,3}$ can be neglected. In this case, the shear overstress is:

$$\bar{\omega} \gg 1 \text{ and } t \gg \tau \quad \Rightarrow \quad [\mathbf{S}_{\mathrm{ov}}]_{12} = 2c_{10}\hat{\alpha} \left( 1 + \frac{\hat{\alpha}^2}{6} \right) \sin(\omega t). \tag{42}$$

This yields to

$$\bar{\omega} \gg 1 \text{ and } t \gg \tau \quad \Rightarrow \quad [\mathbf{S}]_{12} = 2c_{10}\hat{\alpha} \left[ \gamma_{\infty} + \gamma \left( 1 + \frac{\hat{\alpha}^2}{6} \right) \right] \sin(\omega t). \tag{43}$$

Due to the term $\hat{\alpha}^2/6$, the stress amplitude is nonlinearly dependent on the shear amplitude. This phenomenon is not expected for neo-Hookean elasticity. In order to clarify the amplitude dependence, the value 3 is assumed for $\hat{\alpha}$. The amplitudes are calculated with material parameters, listed in Table 4. To focus this analysis on the overstress part, $\gamma_{\infty} = 10^{-4}$ is assumed. Due to the amplitude dependence, the sine amplitude $b_{12,1}/\hat{\alpha}$ converges towards 5MPa (s. Figure 1) at higher angular frequencies. For the chosen material parameter according to neo-Hookean hyperelasticity $b_{12,1}/\hat{\alpha}$ should converge towards $2c_{10} = 2\mathrm{MPa}$ (see Eq. (18)). At high angular

**Table 4** Material parameters for the simulation

| Material parameters for the simulation | | | | |
|---|---|---|---|---|
| $c_{10}$[MPa] | $\gamma_\infty$ | $\gamma_i$ | $\tau$ [s] | $\kappa$[MPa] |
| 1 | $10^{-4}$ | $1-\gamma_\infty$ | 1 | 100 |

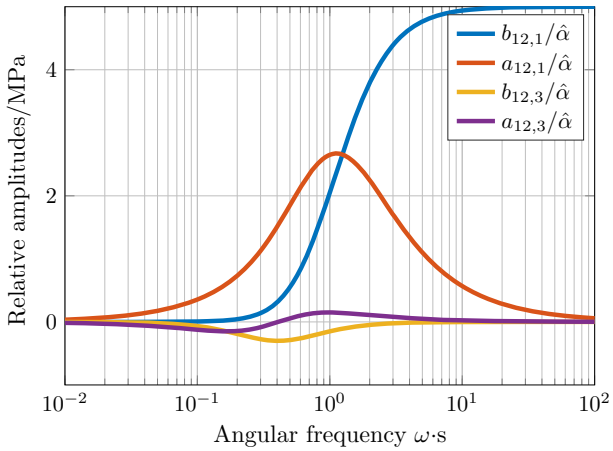


**Fig. 1** Amplitudes of the shear stress $S_{12}$ at $\hat{\alpha} = 3$

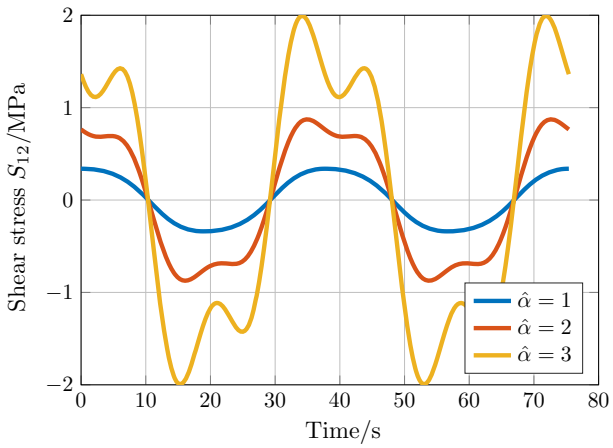


**Fig. 2** Shear stress response for different amplitudes at $\omega = \frac{1}{6}\frac{1}{\text{s}}$

frequencies, it is obvious that $b_{12,1}/\hat{\alpha}$ starts with the expected value $2c_{10} = 2$MPa and converged to the nonlinear amplitude-dependent value. The non-monotonic behaviour of the coefficients $a_{12,3}$, $b_{12,3}$ and the corresponding angular frequency $3\omega$ cannot be neglected in a specific frequency domain and with large shear strain amplitudes $\hat{\alpha} \gg 1$. The cosine amplitude $a_{12,3}$ has a minimum at the angular frequency of $\omega = 1/(\sqrt{6}\text{s})$. The sine amplitude $b_{12,3}$ has a maximum at $\omega = 1/\text{s}$ and a minimum at $\omega = 1/(6\text{s})$. To illustrate the critical frequency range, the shear stress response for an excitation angular frequency of $\omega = 1/(6\text{s})$ is shown in Fig. 2. It is visible that the shear stress response for $\hat{\alpha} = 3$ shows an overshooting behaviour. For smaller amplitudes, this overshooting oscillation can be neglected.

## 2.3 Linearisation relative to a pre-deformed configuration

In most technical applications of rubber bushings, the material is loaded with a pre-deformation. To take this into account, a finite deformation is assumed from the initial configuration $\mathcal{I}$ to the pre-deformed configuration

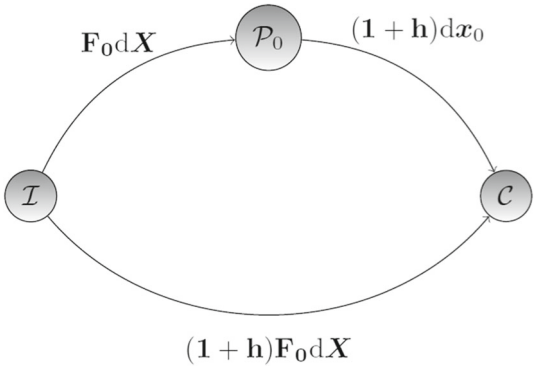


**Fig. 3** Initial, preloaded and current configuration

$\mathcal{P}_0$ (see Fig. 3). The dependency of the viscoelastic behaviour on the pre-deformed configuration is presented with one Maxwell element and neo-Hookean hyperelasticity. A further assumption is that the preload is kept constant for a long time. This means that all overstresses during loading from the initial configuration to the pre-deformed configuration become zero. The deformation change from the pre-deformed configuration to the current configuration is given by $\mathbf{1}+\mathbf{h}$, so that the deformation gradient is

$$\mathbf{F} = (\mathbf{1}+\mathbf{h})\mathbf{F}_0. \tag{44}$$

Herein, $\mathbf{h}$ is the displacement gradient for the referenced pre-deformed configuration. Since the displacement gradient $\|\mathbf{h}\| \ll 1$ is small enough, it is efficient enough to work with the linearised constitutive equations in the pre-deformed configuration. The linearisation can be defined with the Gateaux differential:

$$\delta(\bullet)(\mathbf{x}_0, \mathbf{v}) = \lim_{s\to 0} \frac{(\bullet)(\mathbf{x}_0 + s\mathbf{v}) - (\bullet)(\mathbf{x}_0)}{s}. \tag{45}$$

The linearised form of the weighted Cauchy stress tensor is defined as:

$$\mathbf{S} = \mathbf{S}(\mathbf{F}_0) + \delta\mathbf{S}(\mathbf{F}_0, \mathbf{h}\mathbf{F}_0) \tag{46}$$

For this purpose, the Gateaux differentials of the following variables are needed:

$$\delta J(\mathbf{F}_0, \mathbf{h}\mathbf{F}_0) = J_0^{-1}(\mathbf{1} : \mathbf{h}) \tag{47}$$

$$\delta\left(\mathbf{F}^{-1}\right)(\mathbf{F}_0, \mathbf{h}\mathbf{F}_0) = -\mathbf{F}_0^{-1}\mathbf{h} \tag{48}$$

$$\delta\left(\bar{\mathbf{F}}\right)(\mathbf{F}_0, \mathbf{h}\mathbf{F}_0) = \mathrm{dev}\,[\mathbf{h}]\,\bar{\mathbf{F}}_0 \tag{49}$$

$$\delta\left(\mathbf{C}\right)(\mathbf{F}_0, \mathbf{h}\mathbf{F}_0) = \mathbf{F}_0^T(\mathbf{h}+\mathbf{h}^T)\mathbf{F}_0 \tag{50}$$

$$\delta\left(\bar{\mathbf{C}}\right)(\mathbf{F}_0, \mathbf{h}\mathbf{F}_0) = \bar{\mathbf{F}}_0^T(\mathrm{dev}\left[\mathbf{h}+\mathbf{h}^T\right])\bar{\mathbf{F}}_0 \tag{51}$$

$$\delta\left(\mathbf{C}^{-1}\right)(\mathbf{F}_0, \mathbf{h}\mathbf{F}_0) = -\mathbf{F}_0^{-1}(\mathbf{h}+\mathbf{h}^T)\mathbf{F}_0^{-T} \tag{52}$$

$$\delta\left(\bar{\mathbf{B}}\right)(\mathbf{F}_0, \mathbf{h}\mathbf{F}_0) = \mathrm{dev}\,[\mathbf{h}]\,\bar{\mathbf{B}}_0 + \bar{\mathbf{B}}_0\mathrm{dev}\left[\mathbf{h}^T\right] \quad \text{with} \quad \bar{\mathbf{B}}_0 = \bar{\mathbf{F}}_0\bar{\mathbf{F}}_0^T \tag{53}$$

$$\delta\left(\mathrm{dev}\left[\bar{\mathbf{B}}\right]\right)(\mathbf{F}_0, \mathbf{h}\mathbf{F}_0) = \mathrm{dev}\left[\mathrm{dev}\,[\mathbf{h}]\,\bar{\mathbf{B}}_0 + \bar{\mathbf{B}}_0\mathrm{dev}\left[\mathbf{h}^T\right]\right] \tag{54}$$

For the case of neo-Hookean hyperelasticity (see Table 3), the Gateaux differential of the deviator operator is needed:

$$\begin{aligned}\delta\left(\overline{\mathrm{DEV}}\,[\mathbf{1}]\right)(\mathbf{F}_0, \mathbf{h}\mathbf{F}_0) = &-\frac{2}{3}(\mathbf{1}:\mathbf{h})\overline{\mathrm{DEV}}_0\,[\mathbf{1}] - \frac{1}{3}((\mathbf{h}+\mathbf{h}^T):\bar{\mathbf{B}}_0)\mathbf{C}_0^{-1} \\ &+ \frac{1}{3}(\mathbf{1}:\bar{\mathbf{B}}_0)\mathbf{F}_0^{-1}(\mathbf{h}+\mathbf{h}^T)\mathbf{F}_0^{-T}.\end{aligned} \tag{55}$$

Since the pre-deformation $\mathbf{F}_0$ is constant, the time derivative of the deviator operator is:

$$\frac{\mathrm{d}}{\mathrm{d}t}\left\{\delta\left(\overline{\mathrm{DEV}}\,[\mathbf{1}]\right)(\mathbf{F}_0,\mathbf{h}\mathbf{F}_0)\right\} = -\frac{2}{3}(\mathbf{1}:\dot{\mathbf{h}})\overline{\mathrm{DEV}}_0\,[\mathbf{1}] - \frac{1}{3}((\dot{\mathbf{h}}+\dot{\mathbf{h}}^T):\bar{\mathbf{B}}_0)\mathbf{C}_0^{-1} + \frac{1}{3}(\mathbf{1}:\bar{\mathbf{B}}_0)\mathbf{F}_0^{-1}(\dot{\mathbf{h}}+\dot{\mathbf{h}}^T)\mathbf{F}_0^{-T}. \tag{56}$$

If we assume that all deformations are isochoric for nearly incompressible rubber materials, the Gateaux differential can be reduced to:

$$\frac{\mathrm{d}}{\mathrm{d}t}\left\{\delta\left(\overline{\mathrm{DEV}}\,[\mathbf{1}]\right)(\mathbf{F}_0,\mathbf{h}\mathbf{F}_0)\right\} = -\frac{1}{3}((\dot{\mathbf{h}}+\dot{\mathbf{h}}^T):\bar{\mathbf{B}}_0)\bar{\mathbf{C}}_0^{-1} + \frac{1}{3}(\mathbf{1}:\bar{\mathbf{B}}_0)\bar{\mathbf{F}}_0^{-1}(\dot{\mathbf{h}}+\dot{\mathbf{h}}^T)\bar{\mathbf{F}}_0^{-T}. \tag{57}$$

Herein the condition of incompressibility leads to a unimodular deformation gradient in all configurations and the hydrostatic pressure $p$ has to be defined from the kinematic restriction of incompressibility. With this assumption, the Gateaux differentials of the following variables read as:

$$\delta J(\bar{\mathbf{F}}_0,\mathbf{h}\bar{\mathbf{F}}_0) = 0 = (\mathbf{1}:\mathbf{h}) \Rightarrow \mathrm{dev}\,[\mathbf{h}] = \mathbf{h} \tag{58}$$

$$\delta\left(\bar{\mathbf{F}}^{-1}\right)(\bar{\mathbf{F}}_0,\mathbf{h}\bar{\mathbf{F}}_0) = -\bar{\mathbf{F}}_0^{-1}\mathbf{h} \tag{59}$$

$$\delta\left(\bar{\mathbf{C}}\right)(\bar{\mathbf{F}}_0,\mathbf{h}\bar{\mathbf{F}}_0) = \bar{\mathbf{F}}_0^T(\mathbf{h}+\mathbf{h}^T)\bar{\mathbf{F}}_0 \tag{60}$$

$$\delta\left(\bar{\mathbf{C}}^{-1}\right)(\bar{\mathbf{F}}_0,\mathbf{h}\bar{\mathbf{F}}_0) = -\bar{\mathbf{F}}_0^{-1}(\mathbf{h}+\mathbf{h}^T)\bar{\mathbf{F}}_0^{-T} \tag{61}$$

$$\delta\left(\bar{\mathbf{B}}\right)(\bar{\mathbf{F}}_0,\mathbf{h}\bar{\mathbf{F}}_0) = \mathbf{h}\bar{\mathbf{B}}_0 + \bar{\mathbf{B}}_0\mathbf{h}^T \tag{62}$$

$$\delta\left(\mathrm{dev}\left[\bar{\mathbf{B}}\right]\right)(\bar{\mathbf{F}}_0,\mathbf{h}\bar{\mathbf{F}}_0) = \mathrm{dev}\left[\mathbf{h}\bar{\mathbf{B}}_0 + \bar{\mathbf{B}}_0\mathbf{h}^T\right] \tag{63}$$

$$\frac{\mathrm{d}}{\mathrm{d}t}\left\{\delta\left(\overline{\mathrm{DEV}}\,[\mathbf{1}]\right)(\bar{\mathbf{F}}_0,\mathbf{h}\bar{\mathbf{F}}_0)\right\} = -\frac{1}{3}((\dot{\mathbf{h}}+\dot{\mathbf{h}}^T):\bar{\mathbf{B}}_0)\bar{\mathbf{C}}_0^{-1} + \frac{1}{3}(\mathbf{1}:\bar{\mathbf{B}}_0)\bar{\mathbf{F}}_0^{-1}(\dot{\mathbf{h}}+\dot{\mathbf{h}}^T)\bar{\mathbf{F}}_0^{-T} \tag{64}$$

The linearised weighted overstress is the Gateaux differential of the overstress:

$$\mathbf{S}_{\mathrm{ov}} = \delta\left(\mathrm{dev}\left[\bar{\mathbf{F}}\int_{-\infty}^{t} 2c_{10}e^{-\frac{t-s}{\tau}}\frac{\mathrm{d}}{\mathrm{d}s}\left(\overline{\mathrm{DEV}}\,[\mathbf{1}]\right)\mathrm{d}s\bar{\mathbf{F}}^T\right]\right)(\bar{\mathbf{F}}_0,\mathbf{h}\bar{\mathbf{F}}_0) \tag{65}$$

With the definition in Eq. (45), the linearisation results in

$$\mathbf{S}_{\mathrm{ov}} = \mathrm{dev}\left[\bar{\mathbf{F}}_0\int_{-\infty}^{t} 2c_{10}e^{-\frac{t-s}{\tau}}\delta\left(\frac{\mathrm{d}}{\mathrm{d}s}\left(\overline{\mathrm{DEV}}\,[\mathbf{1}]\right)\right)(\bar{\mathbf{F}}_0,\mathbf{h}\bar{\mathbf{F}}_0)\mathrm{d}s\bar{\mathbf{F}}_0^T\right] \tag{66}$$

Inserting the Gateaux differential from Eq. (64) in (2.3) yields to

$$\mathbf{S}_{\mathrm{ov}} = \mathrm{dev}\left[\int_{-\infty}^{t}\frac{2c_{10}}{3}e^{-\frac{t-s}{\tau}}\left((\mathbf{1}:\bar{\mathbf{B}}_0)(\mathbf{h}'+\left(\mathbf{h}^T\right)') - 2(\mathbf{h}':\bar{\mathbf{B}}_0)\mathbf{1}\right)\mathrm{d}s\right] \tag{67}$$

For the sake of clarity, the differentiation $\frac{\mathrm{d}}{\mathrm{d}s}\mathbf{h}(s)$ is assigned as $\mathbf{h}'$. The linearised weighted overstress is given as:

$$\mathbf{S}_{\mathrm{ov}} = (\mathbf{1}:\bar{\mathbf{B}}_0)\int_{-\infty}^{t}\frac{2c_{10}}{3}e^{-\frac{t-s}{\tau}}\mathrm{dev}\left[\mathbf{h}'+(\mathbf{h}^T)'\right]\mathrm{d}s. \tag{68}$$

Therefore, the linearised weighted Cauchy stress tensor of the total stress is given by:

$$\mathbf{S} = -p\mathbf{1} + \gamma_\infty 2c_{10}\mathrm{dev}\left[\bar{\mathbf{B}}_0 + \mathbf{h}\bar{\mathbf{B}}_0 + \bar{\mathbf{B}}_0\mathbf{h}^T\right] + \gamma(\mathbf{1} : \bar{\mathbf{B}}_0)\int_{-\infty}^{t} \frac{2c_{10}}{3} e^{-\frac{t-s}{\tau}} \mathrm{dev}\left[\mathbf{h}' + (\mathbf{h}^T)'\right] \mathrm{d}s. \tag{69}$$

In the following, the stress response is analysed for a harmonic shear oscillation in the pre-deformed configuration. The total shear strain is:

$$\alpha(t) = \alpha_0 + \Delta\alpha \quad \text{with} \quad \Delta\alpha = \hat{\alpha} e^{\boldsymbol{i}\omega t}. \tag{70}$$

So, the deformation gradient belonging to the pre-deformed configuration is:

$$\bar{\mathbf{F}}_0 = \begin{bmatrix} 1 & \alpha_0 & 0 \\ 0 & 1 & 0 \\ 0 & 0 & 1 \end{bmatrix} \tag{71}$$

and the displacement gradient with respect to pre-deformed configuration is:

$$\mathbf{h} = \begin{bmatrix} 0 & \hat{\alpha} e^{\boldsymbol{i}\omega t} & 0 \\ 0 & 0 & 0 \\ 0 & 0 & 0 \end{bmatrix}. \tag{72}$$

The left Cauchy–Green tensor is:

$$\bar{\mathbf{B}}_0 = \begin{bmatrix} 1+\alpha_0^2 & \alpha_0 & 0 \\ \alpha_0 & 1 & 0 \\ 0 & 0 & 1 \end{bmatrix}. \tag{73}$$

The previously defined total deformation results in the following weighted Cauchy stress:

$$\mathbf{S} = -p\mathbf{1} + \gamma_\infty 2c_{10}\mathrm{dev}\begin{bmatrix} 1+\alpha_0^2+2\alpha_0\Delta\alpha & \alpha_0+\Delta\alpha & 0 \\ \alpha_0+\Delta\alpha & 1 & 0 \\ 0 & 0 & 1 \end{bmatrix} + \gamma(3+\alpha_0^2)\int_0^t \frac{2c_{10}}{3} e^{-\frac{t-s}{\tau}} \mathrm{dev}\begin{bmatrix} 0 & \Delta\alpha' & 0 \\ \Delta\alpha' & 0 & 0 \\ 0 & 0 & 0 \end{bmatrix} \mathrm{d}s, \tag{74}$$

$$\mathbf{S} = -p\mathbf{1} + \gamma_\infty 2c_{10}\begin{bmatrix} \frac{2}{3}\left(\alpha_0^2+2\alpha_0\Delta\alpha\right) & \alpha_0+\Delta\alpha & 0 \\ \alpha_0+\Delta\alpha & -\frac{1}{3}\left(\alpha_0^2+2\alpha_0\Delta\alpha\right) & 0 \\ 0 & 0 & -\frac{1}{3}\left(\alpha_0^2+2\alpha_0\Delta\alpha\right) \end{bmatrix} + \gamma(3+\alpha_0^2)\int_0^t \frac{2c_{10}}{3} e^{-\frac{t-s}{\tau}} \boldsymbol{i}\omega\hat{\alpha} e^{\boldsymbol{i}\omega s}\mathrm{d}s \begin{bmatrix} 0 & 1 & 0 \\ 1 & 0 & 0 \\ 0 & 0 & 0 \end{bmatrix}. \tag{75}$$

The remaining integral is evaluated for the case of a very large time period (i.e. $t \gg \tau$). This yields:

$$\lim_{t\to\infty}\int_0^t e^{-\frac{t-s}{\tau}}\hat{\alpha} e^{\boldsymbol{i}\omega s}\mathrm{d}s = \lim_{t\to\infty}\left(\frac{\tau}{1+\boldsymbol{i}\omega\tau}\left(e^{\boldsymbol{i}\omega t} - e^{-\frac{t}{\tau}}\right)\right) = \frac{\tau}{1+\boldsymbol{i}\omega\tau} e^{\boldsymbol{i}\omega t}. \tag{76}$$

Caused by the boundary condition, the expected Cauchy stress tensor has the form:

$$\mathbf{S} = \mathbf{T} = \begin{bmatrix} 0 & \sigma_{12} & 0 \\ \sigma_{12} & \sigma_n & 0 \\ 0 & 0 & \sigma_n \end{bmatrix}. \tag{77}$$

The three variables to be determined are the shear stress $\sigma_{12}$, the normal stress $\sigma_n$ and the hydrostatic pressure $p$. With the defined response functions (75) and the integration (76), the following system of equations is derived:

$$0 = -p + \gamma_\infty c_{10} \frac{4}{3} \left( \alpha_0^2 + 2\alpha_0 \hat{\alpha} e^{\boldsymbol{i}\omega t} \right), \tag{78}$$

$$\sigma_n = -p - \gamma_\infty c_{10} \frac{2}{3} \left( \alpha_0^2 + 2\alpha_0 \hat{\alpha} e^{\boldsymbol{i}\omega t} \right), \tag{79}$$

$$\sigma_{12} = 2c_{10} \left( \gamma_\infty (\alpha_0 + \hat{\alpha} e^{\boldsymbol{i}\omega t}) + \frac{\gamma}{3} (3 + \alpha_0^2) \frac{\boldsymbol{i}\omega\tau}{1 + \boldsymbol{i}\omega\tau} \hat{\alpha} e^{\boldsymbol{i}\omega t} \right). \tag{80}$$

From Eqs. (78) and (79), the hydrostatic pressure

$$p = \gamma_\infty c_{10} \frac{4}{3} \left( \alpha_0^2 + 2\alpha_0 \hat{\alpha} e^{\boldsymbol{i}\omega t} \right) \tag{81}$$

and the normal stress

$$\sigma_n = -\gamma_\infty 2c_{10} \left( \alpha_0^2 + 2\alpha_0 \hat{\alpha} e^{\boldsymbol{i}\omega t} \right) \tag{82}$$

can be computed. Both consist of a constant component and one that oscillates with the excitation angular frequency. The oscillating part disappears when the static pre-deformation disappears. For the shear stress, the following expression is finally obtained

$$\sigma_{12} = 2c_{10}\gamma_\infty \alpha_0 + 2c_{10}\hat{\alpha} \left( \gamma_\infty + \frac{\gamma}{3} (3 + \alpha_0^2) \frac{\boldsymbol{i}\omega\tau}{1 + \boldsymbol{i}\omega\tau} \right) e^{\boldsymbol{i}\omega t}. \tag{83}$$

The first part is the static shear stress resulting from the static deformation and the second part results from the oscillating additional excitation. The pre-factor before the complex excitation is the complex frequency-dependent modulus consisting of the storage and the loss modulus

$$G^* = 2c_{10} \left( \gamma_\infty + \frac{\gamma}{3} (3 + \alpha_0^2) \frac{\boldsymbol{i}\omega\tau}{1 + \boldsymbol{i}\omega} \right) = G' + \boldsymbol{i} G'' \tag{84}$$

with the storage modulus

$$G' = 2c_{10} \left( \gamma_\infty + \frac{\gamma}{3} (3 + \alpha_0^2) \frac{(\omega\tau)^2}{1 + (\omega\tau)^2} \right) \tag{85}$$

and the loss modulus

$$G'' = 2c_{10} \frac{\gamma}{3} (3 + \alpha_0^2) \frac{(\omega\tau)^2}{1 + (\omega\tau)^2}. \tag{86}$$

Both moduli depend on the pre-deformation in the same way, which does not occur in material models of viscoelasticity based on Maxwell models. In these models, the loss modulus does not depend on the pre-deformation. Experimental investigations in [38] show that the storage modulus decreases with increasing pre-deformation. In the model considered here, the storage modulus increases with increasing pre-deformation. The loss modulus shows the same trend. In Maxwell models, the loss modulus does not depend on the pre-deformations.

### 2.4 Enhanced modification of the Simo model

The analysis of the simple shear shows that the Simo model at high frequency domain differs from the instantaneous stress $\mathbf{S}^{\circ}_{\mathrm{iso}}$. In addition, non-physical overshoots occur. For a relative angular frequency $\bar{\omega} \gg 1$, the differential equation (13) can be approximated by:

$$\dot{\tilde{\mathbf{T}}}_{\mathrm{ov}} \approx \frac{\mathrm{d}}{\mathrm{d}t}\left(\overline{\mathrm{DEV}}\left[\tilde{\mathbf{T}}^{\circ}_{\mathrm{iso}}\right]\right). \tag{87}$$

Since in the free energy Eq. (3) the internal variable $\tilde{\mathbf{T}}_{\mathrm{ov}}$ is scalar multiplied by the unimodular right Cauchy–Green tensor, the deviator operator is applied a second time. In [27], the internal variable in the free energy is multiplied by the right Cauchy–Green tensor. Thus, the deviator operator is only considered in the tensorial differential equation. However, the integration with the deviator operator still leads to non-physical overshoots regarding the neo-Hookean model. In addition, this variant contributes to the volumetric stress components of the Cauchy tensor in the case of isochoric deformations. An alternative would be to consider the unimodular right Cauchy–Green tensor in the free energy, and the differential equation for the internal variable without deviator operator. For the neo-Hookean material model, this leads to the fact that the evolution equation of the internal variable no longer depends on the deformation. If the partial derivative of the free energy is expanded with the inverse right Cauchy–Green tensor, this does not lead to any change in the Cauchy stress tensor. This addition is eliminated again by the deviator operator. The advantage of this addition is that a deformation dependence is taken into account in the evolution equation even with the neo-Hookean model. Another property is that the spontaneous stress tensor becomes $\tilde{\mathbf{T}}^{\circ}_{\mathrm{iso}}(\mathbf{F} = \mathbf{I}) = \mathbf{0}$ also recommended in [7] for the unloaded state. This motivates a suggestion in case of hyperelastic energy functions based on first and second invariants of unimodular right Cauchy–Green tensor. The derived stress relation based on Eq. (11) for an isotropic hyperelastic energy function is:

$$\tilde{\mathbf{T}}^{\circ}_{\mathrm{iso}} = 2\partial_{I_{\bar{\mathbf{C}}}}\bar{W}^{\circ}\mathbf{1} + 2\partial_{II_{\bar{\mathbf{C}}}}\bar{W}^{\circ}(I_{\bar{\mathbf{C}}}\mathbf{1} - \bar{\mathbf{C}}). \tag{88}$$

The following modification is suggested:

$$\tilde{\mathbf{T}}^{\circ}_{\mathrm{iso}} = 2\partial_{I_{\bar{\mathbf{C}}}}\bar{W}^{\circ}(\mathbf{1} - \bar{\mathbf{C}}^{-1}) + 2\partial_{II_{\bar{\mathbf{C}}}}\bar{W}^{\circ}(I_{\bar{\mathbf{C}}}\mathbf{1} - \bar{\mathbf{C}} - 2\bar{\mathbf{C}}^{-1}). \tag{89}$$

This does not affect the thermodynamical consistency and does not change the instantaneous Cauchy stress. With the modified 2nd Piola–Kirchhoff stress tensor, the evolution Eq. (13) can be adapted to:

$$\dot{\tilde{\mathbf{T}}}_{\mathrm{ov}} + \frac{1}{\tau}\tilde{\mathbf{T}}_{\mathrm{ov}} = \frac{\mathrm{d}}{\mathrm{d}t}\tilde{\mathbf{T}}^{\circ}_{\mathrm{iso}} \tag{90}$$

so that the deviatoric operator is only applied once. In this case, the viscoelastic material model based on the neo-Hookean model does not provide overshoots. For very high relative angular frequencies of $\bar{\omega} \gg 1$, the material response is identical to the spontaneous tensor $\mathbf{S}^{\circ}_{\mathrm{iso}}$. Since the deviator operator is applied after the integration of the evolution equation, a clear separation of the volumetric and isochoric stress tensor is ensured. Furthermore, if neo-Hookean energy function is applied, the obtained material model is equal to the proposed material model assigned as "Model A" in [10]. The constitutive equations are summarised in Table 5.

### 2.5 Integration algorithm

In [35, p. 372], an integration algorithm is suggested. In the same manner, the algorithm is summarised in Table 6 for the Simo model. In this section, we assume that the hyperelasticity function for the stored energy depends on the invariants $I_{\bar{\mathbf{C}}}$ and $II_{\bar{\mathbf{C}}}$. The algorithm for the modified model is summarised in Table 7.

## 3 Simulation of a tie rod in car chassis

A tie rod in a multi-link chassis is coupled with the car body and the wheel carrier through two rubber bushings. The bushings of the rod are subjected to torsional loads due to the vertical compression of the car suspension. To show the effects of the presented viscoelastic model, this vertical displacement of a chassis is simulated. A 2D drawing of the tie rod with the relevant dimensions is shown in Fig. 4.

**Table 5** Alternative definition of finite proportional viscoelasticity hyperelasticity

| | |
|---|---|
| *Known or accordingly given functions* | |
| Instantaneous stored isochoric energy | $\bar{W}^{\circ}(\bar{\mathbf{C}})$ |
| Instantaneous stored volumetric energy | $U^{\circ}(J)$ |
| Relaxation function with relative coefficients | $g(t) = \gamma_{\infty} + \sum_{k=1}^{N} \gamma_k e^{-\frac{t}{\tau_k}}$ |
| *Variables, which have to be defined with respect to deformation history* | |
| Alternative instantaneous isochoric 2nd Piola-Kirchhoff stress tensor | $\tilde{\mathbf{T}}^{\circ}_{\text{iso}} = 2\partial_{I_{\bar{\mathbf{C}}}} \bar{W}^{\circ}(\mathbf{1} - \bar{\mathbf{C}}^{-1}) + 2\partial_{II_{\bar{\mathbf{C}}}} \bar{W}^{\circ}(I_{\bar{\mathbf{C}}}\mathbf{1} - \bar{\mathbf{C}} - 2\bar{\mathbf{C}}^{-1})$ |
| Instantaneous isochoric weighted Cauchy stress tensor | $\mathbf{S}^{\circ}_{\text{iso}} = \bar{\mathbf{F}}\tilde{\mathbf{T}}^{\circ}_{\text{iso}}\bar{\mathbf{F}}^{T}$ |
| Overstress of weighted Cauchy stress tensor: | $\mathbf{S}_{\text{ov},k} = \bar{\mathbf{F}} \int_{-\infty}^{t} e^{-\frac{t-s}{\tau_k}} \frac{\mathrm{d}}{\mathrm{d}s}\left(\tilde{\mathbf{T}}^{\circ}_{\text{iso}}\right) \mathrm{d}s \bar{\mathbf{F}}^{T}$ |
| Weighted Cauchy stress tensor: | $\mathbf{S} = J\partial_J U^{\circ}\mathbf{1} + \text{dev}\left[\gamma_{\infty}\mathbf{S}^{\circ}_{\text{iso}} + \sum_{k=1}^{N} \gamma_k \mathbf{S}_{\text{ov},k}\right]$ |

**Table 6** Integration algorithm for finite proportional viscoelasticity [35, p. 372]

| | |
|---|---|
| | *Given entities* |
| Deformation gradient | $\mathbf{F}(t_n) = \mathbf{F}_n$ and $\mathbf{F}(t_{n+1}) = \mathbf{F}_{n+1}$ |
| Internal variable: | $\tilde{\mathbf{T}}_{\text{ov},kn}$ |
| Variables, which have to be defined for the time point $t_{n+1}$ | |
| Relaxation function with relative coefficients: | |
| $g^{*}(\Delta t) = \gamma_{\infty} + \sum_{k=1}^{N} \gamma_k e^{-\frac{\Delta t}{2\tau_k}}$ | |
| Instantaneous isochoric weighted Cauchy stress tensor: | |
| $\mathbf{S}^{\circ}_{\text{iso}n+1} = 2\partial_{I_{\bar{\mathbf{C}}}} \bar{W}^{\circ}(\bar{\mathbf{C}}_{n+1})\bar{\mathbf{B}}_{n+1} + \partial_{II_{\bar{\mathbf{C}}}} \bar{W}^{\circ}(\bar{\mathbf{C}}_{n+1})(I_{\bar{\mathbf{C}}_{n+1}}\bar{\mathbf{B}}_{n+1} - \bar{\mathbf{B}}_{n+1}\bar{\mathbf{B}}_{n+1})$ | |
| $\mathbf{S}^{\circ}_{\text{iso}n} = 2\partial_{I_{\bar{\mathbf{C}}}} \bar{W}^{\circ}(\bar{\mathbf{C}}_{n})\bar{\mathbf{B}}_{n} + \partial_{II_{\bar{\mathbf{C}}}} \bar{W}^{\circ}(\bar{\mathbf{C}}_{n})(I_{\bar{\mathbf{C}}_{n}}\bar{\mathbf{B}}_{n} - \bar{\mathbf{B}}_{n}\bar{\mathbf{B}}_{n})$ | |
| Update algorithmic internal variables: | |
| $\overline{\tilde{\mathbf{T}}_{\text{ov},kn}} = e^{-\frac{\Delta t}{\tau_k}}\tilde{\mathbf{T}}_{\text{ov},kn} - e^{-\frac{\Delta t}{2\tau_k}}\bar{\mathbf{F}}_{n}^{-1}\text{dev}\left[\mathbf{S}^{\circ}_{\text{iso}n}\right]\bar{\mathbf{F}}_{n}^{-T}$ | |
| $\tilde{\mathbf{T}}_{\text{ov},kn+1} = \overline{\tilde{\mathbf{T}}_{\text{ov},kn}} + e^{-\frac{\Delta t}{2\tau_k}}\bar{\mathbf{F}}_{n+1}^{-1}\text{dev}\left[\mathbf{S}^{\circ}_{\text{iso}n+1}\right]\bar{\mathbf{F}}_{n+1}^{-T}$ | |
| $\overline{\mathbf{S}_{\text{ov},kn}} = \bar{\mathbf{F}}_{n+1}\overline{\tilde{\mathbf{T}}_{\text{ov},kn}}\bar{\mathbf{F}}_{n+1}^{T}$ | |
| Weighted Cauchy stress tensor: | |
| $\mathbf{S} = J_{n+1}\partial_J U^{\circ}(J_{n+1})\mathbf{1} + \text{dev}\left[g^{*}(\Delta t)\mathbf{S}^{\circ}_{\text{iso}n+1} + \sum_{k=1}^{N} \gamma_k \overline{\mathbf{S}_{\text{ov},kn}}\right]$ | |

The simulation is performed using the FEM software Abaqus. Before setting up the boundary conditions, the tie rod geometry is discritised with 3D elements. The rubber part is discretised by 10976 C3D8H (8-node linear brick, hybrid with constant pressure) elements, while the steel part is discretised by 23624 C3D8R (8-node linear brick, reduced integration with hourglass control) elements. Figure 5 shows the discretisation of the complete geometry.

After discretisation, the boundary conditions are set as shown in Fig. 6. Two reference points are kinematically coupled with the inner diameters of the rubber bushings. The displacement of the reference point 1 (RP1) is kept fixed in all directions except the rotational displacement around the x-axis, which is set free. On the other end of the rod, the reference point 2 (RP2) is allowed to displace in the z- and the y-direction and rotate about the x-axis. All other displacement boundary conditions are held fixed. The displacement in the z-direction is given as:

$$U_z = U_{z0} + \hat{U}_z \sin(\omega t). \tag{91}$$

To highlight the non-physical response of the presented model, four different loading cases are simulated. The loading cases are summarised in Table 8. The results are obtained for both the presented model (Abaqus Model for finite viscoelasticity) and the modified model. The implementation of the modified model in Abaqus is done through a user material subroutine (UMAT) programmed using Fortran 77.

The values of material parameters for the rubber bushings are listed in Table 4. The steel rod has a Young's modulus (E) of 210 GPa and a Poisson's ratio ($\nu$) of 0.3. The neo-Hookean solid is used for modelling the

**Table 7** Integration algorithm for alternate model suggested in sec. 2.4

*Given entities*

Deformation gradient: $\mathbf{F}(t_n) = \mathbf{F}_n$ and $\mathbf{F}(t_{n+1}) = \mathbf{F}_{n+1}$

Internal variable: $\tilde{\mathbf{T}}_{\mathrm{ov},kn}$

Variables, Which have to be defined for the time point $t_{n+1}$

Relaxation function with relative coefficients:

$$g^*(\Delta t) = \gamma_\infty + \sum_{k=1}^{N} \gamma_k e^{-\frac{\Delta t}{2\tau_k}}$$

Instantaneous isochoric weighted Cauchy stress tensor:

$$\begin{aligned}\mathbf{S}^{\circ}_{\mathrm{iso}n+1} &= 2\partial_{I_{\bar{\mathbf{C}}}} \bar{W}^{\circ}(\bar{\mathbf{C}}_{n+1})(\bar{\mathbf{B}}_{n+1} - \mathbf{1}) \\ &\quad + \partial_{II_{\bar{\mathbf{C}}}} \bar{W}^{\circ}(\bar{\mathbf{C}}_{n+1})(I_{\bar{\mathbf{C}}_{n+1}} \bar{\mathbf{B}}_{n+1} - \bar{\mathbf{B}}_{n+1}\bar{\mathbf{B}}_{n+1} - 2 \cdot \mathbf{1}) \\ \mathbf{S}^{\circ}_{\mathrm{iso}n} &= 2\partial_{I_{\bar{\mathbf{C}}}} \bar{W}^{\circ}(\bar{\mathbf{C}}_{n})(\bar{\mathbf{B}}_{n} - \mathbf{1}) \\ &\quad + \partial_{II_{\bar{\mathbf{C}}}} \bar{W}^{\circ}(\bar{\mathbf{C}}_{n})(I_{\bar{\mathbf{C}}_{n}} \bar{\mathbf{B}}_{n} - \bar{\mathbf{B}}_{n}\bar{\mathbf{B}}_{n} - 2 \cdot \mathbf{1})\end{aligned}$$

Update algorithmic internal variables:

$$\begin{aligned}\overline{\tilde{\mathbf{T}}_{\mathrm{ov},kn}} &= e^{-\frac{\Delta t}{\tau_k}} \tilde{\mathbf{T}}_{\mathrm{ov},kn} - e^{-\frac{\Delta t}{2\tau_k}} \bar{\mathbf{F}}_n^{-1} \mathbf{S}^{\circ}_{\mathrm{iso}n} \bar{\mathbf{F}}_n^{-T} \\ \tilde{\mathbf{T}}_{\mathrm{ov},kn+1} &= \overline{\tilde{\mathbf{T}}_{\mathrm{ov},kn}} + e^{-\frac{\Delta t}{2\tau_k}} \bar{\mathbf{F}}_{n+1}^{-1} \mathbf{S}^{\circ}_{\mathrm{iso}n+1} \bar{\mathbf{F}}_{n+1}^{-T} \\ \overline{\mathbf{S}_{\mathrm{ov},kn}} &= \bar{\mathbf{F}}_{n+1} \overline{\tilde{\mathbf{T}}_{\mathrm{ov},kn}} \bar{\mathbf{F}}_{n+1}^{T}\end{aligned}$$

Weighted Cauchy stress tensor:

$$\mathbf{S} = J_{n+1}\partial_J U^{\circ}(J_{n+1})\mathbf{1} + \mathrm{dev}\left[g^*(\Delta t)\mathbf{S}^{\circ}_{\mathrm{iso}n+1} + \textstyle\sum_{k=1}^{N} \gamma_k \overline{\mathbf{S}_{\mathrm{ov},kn}}\right]$$

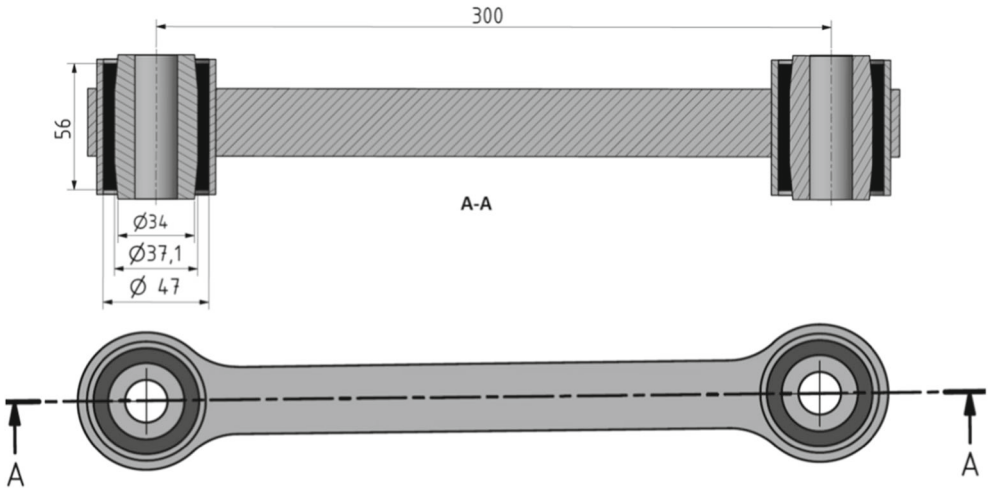


**Fig. 4** A 2D drawing with the dimensions of the modelled tie rod

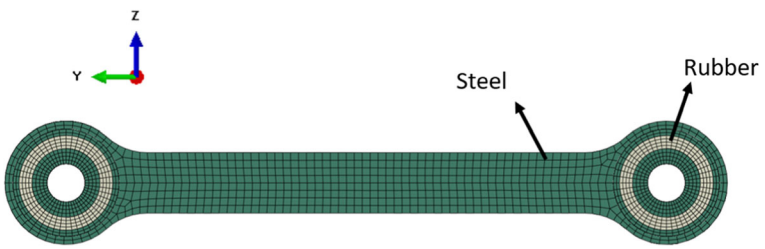


**Fig. 5** The discretised 3D Model


**Fig. 6** Boundary conditions for the simulation

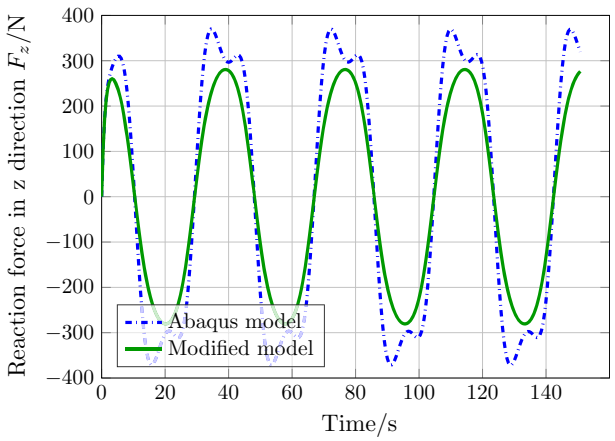


**Fig. 7** Calculated reaction force $F_z(U_Z)$ as a function of time for both models at 130 mm amplitude loading

**Table 8** Simulation cases

| Simulation cases | | | |
|---|---|---|---|
| Load case | Amplitude $\hat{U}_z$ [mm] | Angular frequency $\omega$ [rad/sec] | Preload $U_{z0}$ [mm] |
| LC1 | 130 | 1/6 | 0 |
| LC2 | 1 | $20\pi$ | 0 |
| LC3 | 1 | $20\pi$ | 100 |
| LC4 | 130 | $20\pi$ | 0 |

hyperelastic parts of the model. The parameter values are purposefully chosen so that the material response has a very small equilibrium stress ($\gamma_\infty$ has a very small value).

### 3.1 Simulation of an alternating finite deformation

In this subsection, the first simulation case (LC1) along with its results is presented. As shown in Fig. 7, the loading is applied in the z-direction as a sine function with an amplitude of 130 mm (see. Equation (91) and LC1 from Table 8). The reaction force in the z-direction is plotted against time in Fig. 7. As a response to the sinusoidal deformation, the reaction forces are expected to behave also in a sinusoidal manner. Figure 7 shows,

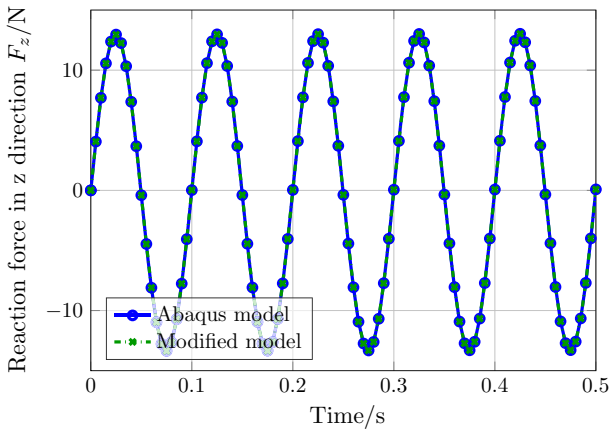


**Fig. 8** Calculated reaction force $F_z(U_Z)$ as a function of time for both models at 1 mm amplitude loading with no preload deformation

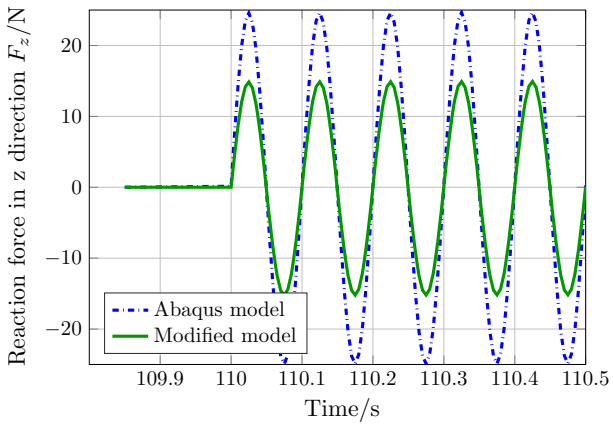


**Fig. 9** Calculated reaction force $F_z(U_Z)$ as a function of time for both models at 1 mm amplitude loading with preload deformation of 100 mm

on the contrary, a non-physical response of the original Abaqus model. Instead, the modified model shows the expected behaviour of a sinusoidal wave form of the reaction force.

## 3.2 Preload dependency of models

As discussed and shown in Sect. 2.3, the dynamic behaviour of the model should not depend on the applied static preload. To show the preload dependency of the Abaqus model, two different loading cases are simulated (LC2 and LC3 from Table 8). In LC2, no pre-deformation is applied. A cyclic loading with an amplitude of 1 mm and an angular frequency of $20\pi$/sec is simulated. The results are shown in Fig. 8.

The results show that at the small amplitude with no pre-deformation, the behaviour of the two models, the Abaqus model, and the modified model, are identical. Adding a preload before cyclic deformation (LC3) shows the pre-load dependency of the Abaqus model as visualised in Fig. 9. In LC3, the preload is set to 100 mm. Before applying the cyclic loading, the material pre-deformation is held constant for 100 s to allow complete relaxation of the stresses. After ensuring a complete relaxation where the reaction forces are zero, a cyclic deformation is applied with an amplitude of 1 mm and an angular frequency of $20\pi$/sec. In Fig. 9, the force response to the vertical displacement is shown. It is obvious that the reaction force with the Abaqus model is nearly two times greater than the reaction with the modified model.

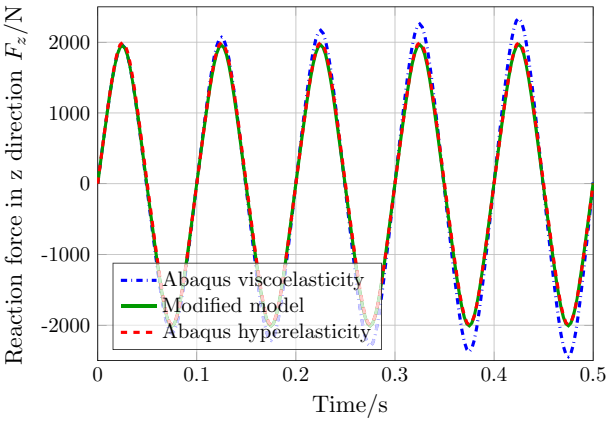


**Fig. 10** Calculated reaction force $F_z(U_Z)$ as a function of time for both models at 130 mm amplitude loading with loading frequency of 10 Hz ($\omega = 2\pi$ rad/sec)

### 3.3 Model behaviour at high frequency loading

According to the Maxwell model, the material responds at high frequency loading with the instantaneous elasticity. That means that at a sufficiently high frequency, the response is mainly elastic. The results obtained by using the Abaqus model for hyperelasticity without adding viscous effects should be, therefore, at high frequencies identical to the results obtained using the Abaqus model with adding one viscoelastic arm. In the simulation case LC4, the results of the three models (Abaqus finite viscoelasticity, modified model, and Abaqus model for hyperelasticity) are compared as shown in Fig. 10.

The results from the hyperelastic model of Abaqus are the same as those obtained from the modified model. Moreover, the finite viscoelastic model of Abaqus shows a sine wave with an increasing amplitude which is a non-physical response.

## 4 Conclusion

The use of commercial FEA software in the industrial field requires prior knowledge of the limitations of the implemented material models. In this contribution, the focus was on testing the behaviour of the Simo model for finite viscoelasticity under different loading conditions. For this purpose, an analytical stress response for a simple shear load is derived in Sect. 2. The analytical investigations show that the applied viscoelastic material model suggested in [3] shows non-physical overshoot oscillations in a specific frequency range. Furthermore, for relatively high frequencies the stress amplitude depends nonlinearly on the shear amplitude. The linearisation in the pre-deformed configuration shows that the storage modulus increases with increasing pre-deformation. Experimental results show a reverse phenomenon, i.e. decreasing storage modulus with increasing pre-deformation. The loss modulus also increases with increasing pre-deformation. To avoid these undesirable phenomena, a modified model is suggested. For the implementation of the modified model, the existing integration algorithm can be adjusted with minor changes.

Finally, an example of an application is chosen to illustrate the difference between the modified and the existing Simo model. The chosen example is a tie rod in a multi-link chassis. The compression of the chassis leads to a torsional load on the rubber bearings. With the Simo model, a non-physical overshoot oscillation can be shown in the vertical reaction force. Furthermore, the analytical results from the linearisation could be shown for the chosen example with load case LC2 and LC3. With the last load case (LC4), it is shown that the desired behaviour of the Simo model, i.e. proportional overstress at high frequencies, is only satisfied for small deformations. All of these effects can be avoided with the suggested modification. It should be mentioned that these effects only make a visible contribution in the case of large deformations.

The modification is implemented into Abaqus for neo-Hookean hyperelasticity. It has to be shown that the modification avoids these effects also with other hyperelastic models. It is expected that with higher-order hyperelastic models, the overshoot cannot be avoided even with the modification. But the desired proportionality of the overstress at higher frequencies should be ensured with the modification.

**Funding** Open Access funding enabled and organized by Projekt DEAL.

## References

1. Fung, Y.-C.: Biomechanics: Mechanical Properties of Living Tissues, 2nd edn. Springer, New York (2013)
2. Pipkin, A.C., Rogers, T.G.: A non-linear integral representation for viscoelastic behaviour. J. Mech. Phys. Solids **16**(1), 59–72 (1968). https://doi.org/10.1016/0022-5096(68)90016-1
3. Simo, J.C.: On a fully three-dimensional finite-strain viscoelastic damage model formulation and computational aspects. Comput. Methods Appl. Mech. Eng. **60**, 153–173 (1987)
4. Ciambella, J., Destrade, M., Ogden, R.W.: On the ABAQUS FEA model of finite viscoelasticity. Rubber Chem. Technol. **82**(2), 184–193 (2009). https://doi.org/10.5254/1.3548243
5. Simulia: Abaqus/theory guide. Dassault Systèmes Simulia Corp (2018)
6. Baaser, H.: On dissipation in viscoelastic material models. In: 9th Rubber Fall Colloquium (2010)
7. De Pascalis, R., Abrahams, I.D., Parnell, W.J.: On nonlinear viscoelastic deformations: a reappraisal of Fung's quasi-linear viscoelastic model. Proc. Royal Soc. Mathemat. Phys. Eng. Sci. **470**(2166), 20140058 (2014). https://doi.org/10.1098/rspa.2014.0058
8. Lion, A.: A physically based method to represent the thermo-mechanical behaviour of elastomers. Acta Mech. **123**, 1–25 (1997). https://doi.org/10.1007/BF01178397
9. Reese, S., Govindjee, S.: A theory of finite viscoelasticity and numerical aspects. Int. J. Solids Structures **35**, 3455–3482 (1998)
10. Haupt, P., Lion, A.: On finite linear viscoelasticity of incompressible isotropic materials. Acta Mech. **159**, 87–124 (2002). https://doi.org/10.1007/BF01171450
11. Lion, A., Höfer, P.: On the phenomenological representation of curing phenomena in continuum mechanics. Arch. Mech. **59**, 59–89 (2007)
12. Yagimli, B., Lion, A.: Experimental investigations and material modelling of curing processes under small deformations. ZAMM - J. Appl. Mathemat. Mech. / Zeitschrift für Angewandte Mathematik und Mechanik **91**, 342–359 (2011). https://doi.org/10.1002/zamm.201000096
13. Yagimli, B.: Kontinuumsmechanische betrachtung von aushärtevorgängen: Experimente, thermomechanische materialmodellierung und numerische umsetzung. PhD thesis, Universität der Bundeswehr München (2013)
14. Johlitz, M., Dippel, B., Lion, A.: Dissipative heating of elastomers: a new modelling approach based on finite and coupled thermomechanics. Continuum Mech. Thermodyn. **28**(4), 1111–1125 (2016). https://doi.org/10.1007/s00161-015-0469-7
15. Schröder, J., Lion, A., Johlitz, M.: Numerical studies on the self-heating phenomenon of elastomers based on finite thermo-viscoelasticity. J. Rubber Res. **24**(2), 237–248 (2021). https://doi.org/10.1007/s42464-021-00089-5. Accessed March 17, 2022
16. Besdo, D., Ihlemann, J.: A phenomenological constitutive model for rubberlike materials and its numerical applicatoins. Int. J. Plast **19**, 1019–1036 (2003)
17. Juhre, D., Doniga-Crivat, M., Ihlemann, J.: The influence of inelasticity on the lifetime of filled elastomers under multiaxial loading conditions. Constitutive Model Rubber VII-Proc, 359 (2011)
18. Weiser, S., Lehmann, T., Landgraf, R., Goldberg, N., Donner, H., Ihlemann, J.: Experimental and numerical analysis of cord-elastomer composites. J. Rubber Res. **24**(2), 211–225 (2021). https://doi.org/10.1007/s42464-021-00091-x. Accessed Nov 29, 2022
19. Reese, S.: A micromechanically motivated material model for the thermo-viscoelastic material behaviour of rubber-like polymers. Int. J. Plast **19**(7), 909–940 (2003). https://doi.org/10.1016/S0749-6419(02)00086-4
20. Miehe, C., Göktepe, S., Lulei, F.: A micro-macro approach to rubber-like materials-Part I: the non-affine micro-sphere model of rubber elasticity. J. Mech. Phys. Solids **52**(11), 2617–2660 (2004). https://doi.org/10.1016/j.jmps.2004.03.011
21. Raghunath, R., Juhre, D., Klüppel, M.: A physically motivated model for filled elastomers including strain rate and amplitude dependency in finite viscoelasticity. Int. J. Plast **78**, 223–241 (2016). https://doi.org/10.1016/j.ijplas.2015.11.005
22. Freund, M., Ihlemann, J.: Generalization of one-dimensional material models for the finite element method. ZAMM-J. Appl. Mathemat. Mech./Zeitschrift für Angewandte Mathematik und Mechanik: Applied Mathematics and Mechanics **90**(5), 399–417 (2010)
23. Plagge, J., Ricker, A., Kröger, N., Wriggers, P., Klüppel, M.: Efficient modeling of filled rubber assuming stress-induced microscopic restructurization. Int. J. Eng. Sci. **151**, 103291 (2020)
24. Dal, H., Gültekin, O., Açıkgöz, K.: An extended eight-chain model for hyperelastic and finite viscoelastic response of rubberlike materials: Theory, experiments and numerical aspects. J. Mech. Phys. Solids **145**, 104159 (2020). https://doi.org/10.1016/j.jmps.2020.104159
25. Arruda, E.M., Boyce, M.C.: A three-dimensional constitutive model for the large stretch behavior of rubber elastic materials. J. Mech. Phys. Solids **41**(2), 389–412 (1993). https://doi.org/10.1016/0022-5096(93)90013-6
26. Boltzmann, L.: Zur Theorie der elastischen Nachwirkung. Akad. Wiss. Wien **70**, 275–306 (1874)
27. Behnke, R., Kaliske, M.: Thermo-mechanically coupled investigation of steady state rolling tires by numerical simulation and experiment. Int. J. Non-Linear Mech. **68**, 101–131 (2015). https://doi.org/10.1016/j.ijnonlinmec.2014.06.014. (**Mechanics of Rubber - in Memory of Alan Gent**)

28. Berjamin, H., Destrade, M., Parnell, W.J.: On the thermodynamic consistency of quasi-linear viscoelastic models for soft solids. Mech. Res. Commun. **111**, 103648 (2021)
29. Berjamin, H., De Pascalis, R.: Acoustoelastic analysis of soft viscoelastic solids with application to pre-stressed phononic crystals. Int. J. Solids Struct. **241**, 111529 (2022). https://doi.org/10.1016/j.ijsolstr.2022.111529
30. Rashid, B., Destrade, M., Gilchrist, M.D.: Mechanical characterization of brain tissue in simple shear at dynamic strain rates. J. Mech. Behav. Biomed. Mater. **28**, 71–85 (2013)
31. Lucas, S.R., Bass, C.R., Salzar, R.S., Oyen, M.L., Planchak, C., Ziemba, A., Shender, B.S., Paskoff, G.: Viscoelastic properties of the cervical spinal ligaments under fast strain-rate deformations. Acta Biomater. **4**(1), 117–125 (2008). https://doi.org/10.1016/j.actbio.2007.08.003
32. Destrade, M., Murphy, J.G., Saccomandi, G.: Simple shear is not so simple. Int. J. Non-Linear Mech. **47**(2), 210–214 (2012). https://doi.org/10.1016/j.ijnonlinmec.2011.05.008. (**Nonlinear Continuum Theories**)
33. Anssari-Benam, A., Horgan, C.O.: On modelling simple shear for isotropic incompressible rubber-like materials. J. Elast. **147**(1), 83–111 (2021). https://doi.org/10.1007/s10659-021-09869-x
34. Cwiekala, N., Traphöner, H., Haupt, P., Clausmeyer, T., Tekkaya, A.E.: Analytical model of the in-plane torsion test. Acta Mech. **233**(2), 641–663 (2022). https://doi.org/10.1007/s00707-021-03129-8
35. Simo, J.C., Hughes, T.J.R.: Computational Inelasticity: Mechanics and Materials. Springer, New York (1998)
36. Flory, P.J.: Thermodynamic relations for high elastic materials. Trans. Faraday Soc. **57**, 829–838 (1961). https://doi.org/10.1039/TF9615700829
37. Clayton, J.D., Freed, A.D.: A constitutive framework for finite viscoelasticity and damage based on the Gram-Schmidt decomposition. Acta Mech. **231**(8), 3319–3362 (2020). https://doi.org/10.1007/s00707-020-02689-5
38. Wollscheid, D., Lion, A.: Predeformation- and frequency-dependent material behaviour of filler-reinforced rubber: Experiments, constitutive modelling and parameter identification. Int. J. Solids Struct. **50**(9), 1217–1225 (2013). https://doi.org/10.1016/j.ijsolstr.2012.12.015